AD-A088 739 TEL-AVIV UNIV (ISRAEL) SCHOOL OF ENGINEERING F/G 20/5
INTERACTION OF ELECTRONS AND ELECTROMAGNETIC WAVES IN PERIODIC --ETC(U)
FEB 79 A GROVER AFOSR-77-3445

UNCLASSIFIED AFOSR-TR-80-0690 NL

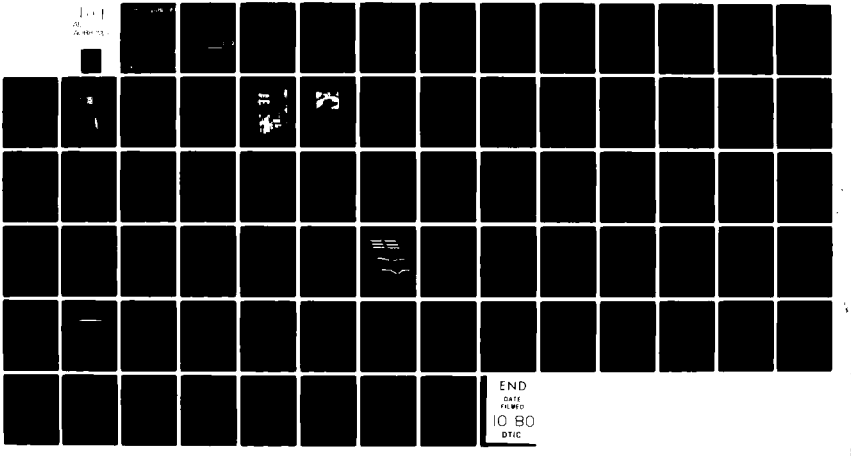

END
DATE FILMED
10 80
DTIC

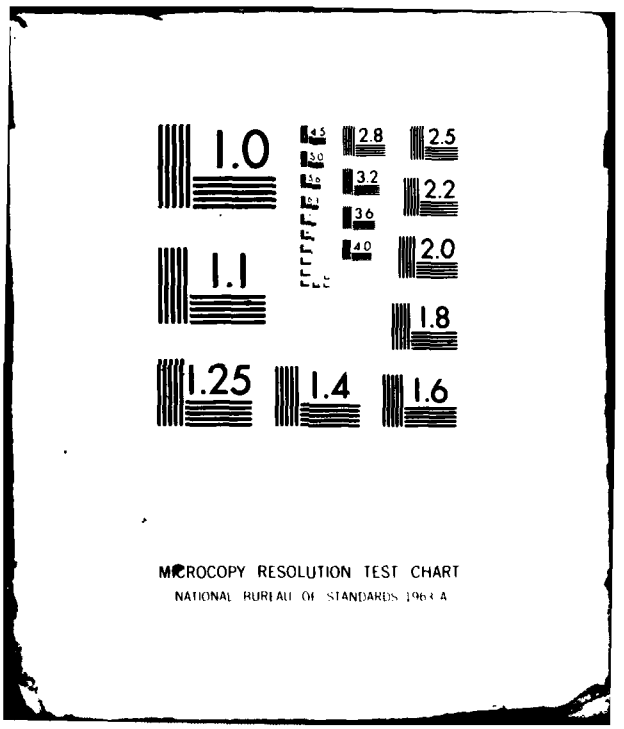
1.0
1.1
1.25
1.4
1.6
1.8
2.0
2.2
2.5
2.8
3.2
3.6
4.0
MICROCOPY RESOLUTION TEST CHART
NATIONAL BUREAU OF STANDARDS 1963 A

LEVEL II

AD A088739

SCHOOL OF ENGINEERING
TEL-AVIV UNIVERSITY
Tel-Aviv, Israel

DTIC
ELECTE
SEP 4 1980
S
D

Approved for public release;
distribution unlimited.

DDC FILE COPY

80 9 2 05

LEVEL II

9

Principal investigator:

Avraham Gover

Tel-Aviv University School of Engineering

Tel-Aviv, Israel

24 February 1979

Grant Number: AFOSR 77-3445

INTERACTION OF ELECTRONS AND ELECTROMAGNETIC WAVES IN PERIODIC STRUCTURES

Final
Progress Report 1 Oct. 1978 - 30 Sept. 1979

Prepared for

AIR FORCE OFFICE OF SCIENTIFIC RESEARCH AND DEVELOPMENT

Bolling AFB, Washington D.C., U.S.A.

and

EUROPEAN OFFICE OF AEROSPACE RESEARCH AND DEVELOPMENT

London, England.

UNCLASSIFIED

SECURITY CLASSIFICATION OF THIS PAGE (When Data Entered)

REPORT DOCUMENTATION PAGE	READ INSTRUCTIONS BEFORE COMPLETING FORM
1. REPORT NUMBER (18) AFOSR-TR- 80-0690 (19)	2. GOVT ACCESSION NO. AD-A088 739	3. RECIPIENT'S CATALOG NUMBER
4. TITLE (and Subtitle) INTERACTION OF ELECTRONS AND ELECTROMAGNETIC WAVES IN PERIODIC STRUCTURES.	5. TYPE OF REPORT & PERIOD COVERED Final
	6. PERFORMING ORG. REPORT NUMBER
7. AUTHOR(s) (10) Avraham Gover (15)	8. CONTRACT OR GRANT NUMBER(s) AFOSR-77-3445
9. PERFORMING ORGANIZATION NAME AND ADDRESS School of Engineering Tel-Aviv University Tel-Aviv, Israel.	10. PROGRAM ELEMENT, PROJECT, TASK AREA & WORK UNIT NUMBERS 61102F (16) 2301/A1 (17) A1
11. CONTROLLING OFFICE NAME AND ADDRESS AFOSR/NP Bolling AFB, Bldg. #410 Wash DC 20332	12. REPORT DATE (11) Feb 79
	13. NUMBER OF PAGES 75
14. MONITORING AGENCY NAME & ADDRESS (if different from Controlling Office) (9) Final progress Rept. 1 Oct 78-30 Sep 79	15. SECURITY CLASS. (of this report) unclassified
	15a. DECLASSIFICATION/DOWNGRADING SCHEDULE

16. DISTRIBUTION STATEMENT (of this Report)

Approved for public release; distribution unlimited.

17. DISTRIBUTION STATEMENT (of the abstract entered in Block 20, if different from Report)

18. SUPPLEMENTARY NOTES

19. KEY WORDS (Continue on reverse side if necessary and identify by block number)

20. ABSTRACT (Continue on reverse side if necessary and identify by block number)

Theoretical work on free electron lasers (FEL) proposed new mechanisms for FELs, developed numerical computational tools for electron gun design, continued optical experiments, completed the design and initial fabrication of two versions of electron guns and made appreciable progress in the construction of an experimental set-up for spontaneous and stimulated Cerenkov-Smith Purcell experiments.

DD FORM 1 JAN 73 1473 EDITION OF 1 NOV 65 IS OBSOLETE UNCLASSIFIED 407500

Introduction

This progress report summarizes progress in a research program sponsored under Grant no. 77-3445 during the period 1 Oct. 1978 - 30 Sept. 1979. The main purpose of this report is to inform the program managers in charge of this program in AFOSR and EOARD on the progress in research achieved during this year as well as difficulties faced. The report was written in a somewhat extended form in order to summarize and keep a record on different results obtained during this research year. This is in order to serve our research group and people associated with our research program as a useful reference and information source.

I. Summary of Scientific Work

During the second year of research sponsored under grant no. 77-3444 we have further developed theoretical work on free electron lasers (FEL), proposed new mechanisms for FELs, developed numerical computational tools for electron gun design, continued optical experiments, completed the design and initial fabrication of two versions of electron guns and made appreciable progress in the construction of an experimental set-up for spontaneous and stimulated Cerenkov-Smith-Purcell experiments, shown schematically in Fig. 1.

Analitical Work

A new kind of FEL mechanism based on longitudinal electrostatic bremsstrahlung was proposed and analyzed in two publications[1,2] which are enclosed. The mechanism is based on a longitudinal periodic electrostatic field which periodically accelerate-decelerate the electron beam which can then interact with the longitudinal electric field component of a TM electromagnetic mode. This kind of interaction has certain similarities with magnetic bremsstrahlung lasers as $\omega \simeq 1$ as with Cerenkov-Smith-Purcell lasers. The basic scheme is shown in Fig. 2. An invention disclosure on this scheme was submitted to AFOSR on April 1979.

In another paper which was submitted for publication,[3] an "accurate" analysis of magnetic bremsstrahlung FEL was derived in the low gain regime for a general momentum distribution of electrons in the electron beam and

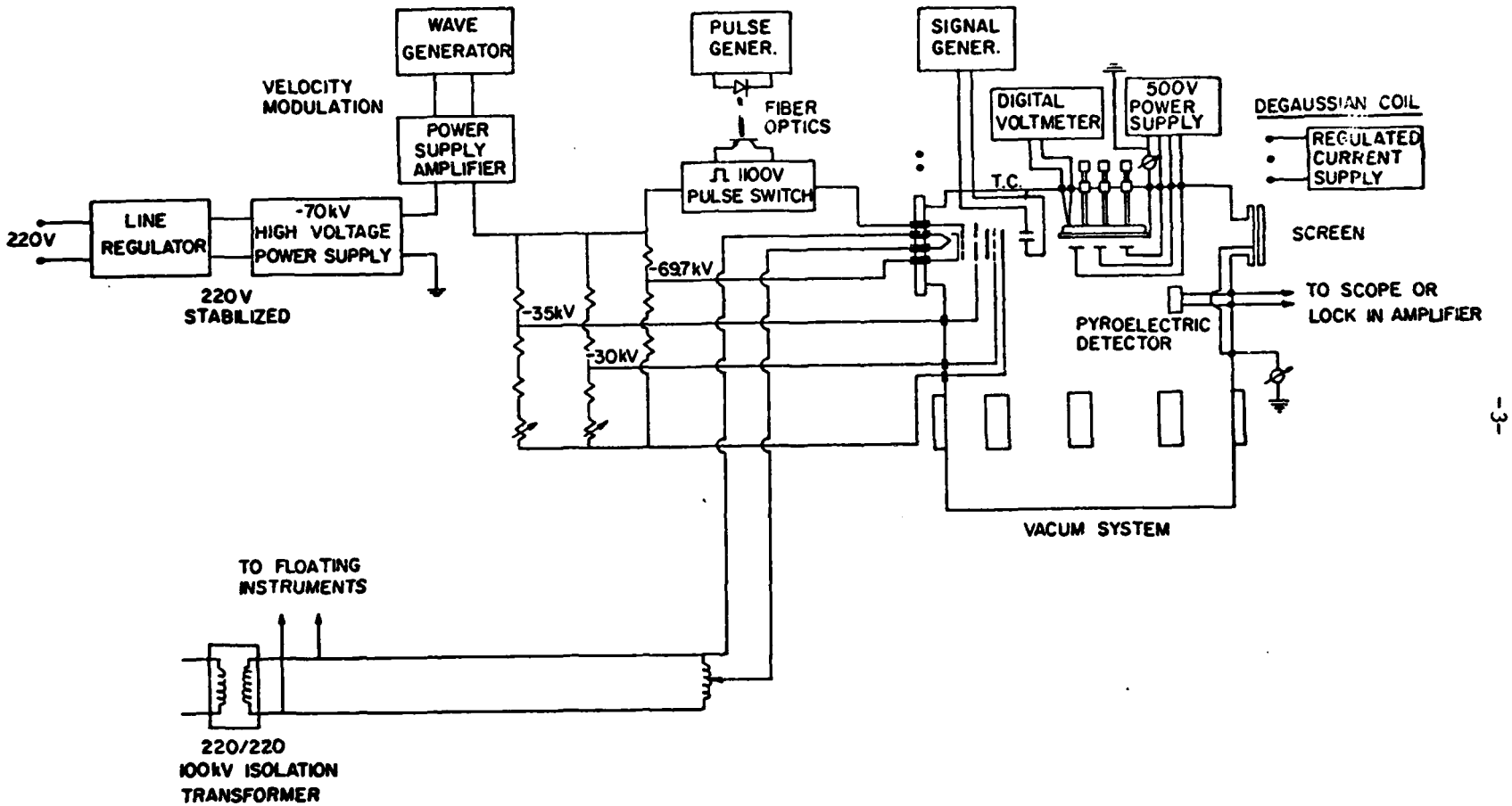

Fig. 1: A schematic description of a Smith-Purcell-Cerenkov experimental set-up.

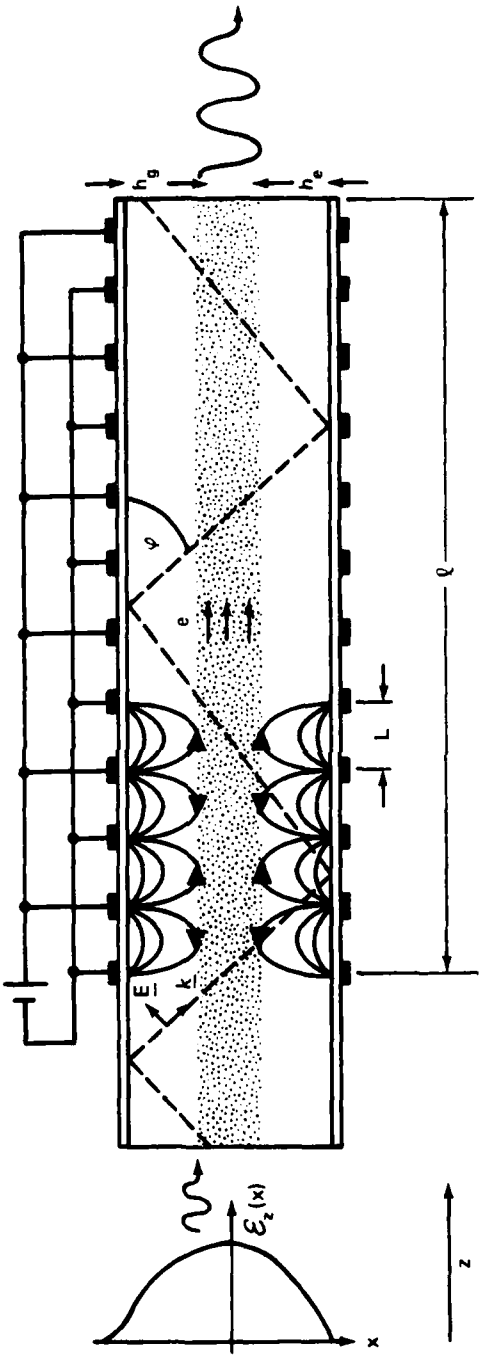

Fig. 2: A scheme of a longitudinal electrostatic bremsstrahlung FEL.

for a general longitudinal spatial variation of the magnetic pump field. This analysis was used to examine the effect of transverse electron velocity spread and of irregularities in the periodic pump field on the FEL gain. This work was done during a collaborative research work with P. Sprangle and V. Granatstein from N.R.L., Washington D.C.

An important theoretical development which was achieved in the last year is the derivation of a unified comprehensive model for all kinds of FEL (including Cerenkov, Smith-Purcell, Magnetic and electrostatic bremsstrahlung and stimulated Compton-Raman scattering). It was shown that all of these FELs obey similar dispersion relations. Their various operation parameters (gain, efficiency, power, linewidth) were analized and compared for different FELs. This work was also done in part in collaboration with P. Sprangle. It is being now prepared for publication.

Electron Gun Design

During the reported period we hosted Dr. Kurt Amboss from Hughs Aircraft Electron Tube Div. in Torrance Cal. Dr. Amboss stayed in Tel-Aviv University as a guest professor for one school semester and taught a graduate course in electron optics. This was an excellent way to introduce our research group to the art of electron gun design which is an important part in free electron lasers development.

Dr. Amboss has designed for the experiment a thin sheet beam electron gun which is designed to operate with the following parameters (electron gun no. 2):

Beam voltage : 50-70 KV

Current density: 0.1 - 1 A/cm^2

Beam thickness : 10 μm

Beam width : 100-1000 μm

Circuit length : 2-10 cm

Beam current : 1-100 μA

The design details and considerations are explained in Appendix A. The electron design is shown in Fig. A-3 and an artist concept of it is shown in Fig. A-7.

Besides the invaluable contribution of Dr. Amboss we have used from time to time the consulting services of Eng. A. Eichenbaum, head of research and development in the electron tubes plant of Elta Avionic Industry in Ashdod. A. Eichenbaum has long experience in electron tubes and electron optics which he accumulated in his present position and previously in RCA Laboratories. His advise on electronic materials, preliminary electron-optical designs and providing a computer program for electron gun design have been very valuable.

Numerical Analysis

During this year we have adapted and put into work an important design tool which is useful for our electron gun design and construction work. This is a computer program which solves for the electron trajectories under general boundary conditions (with cylindrical or planar symmetry) including

space charge effects. This program is based on SLAC's electron optics code which was written originally for an IBM 370 computer and needed some more work and adaptation to be used in our CDC 6800 computer and fit our special design requirements (see details in Appendix B). This adaptation was carried out by a research assistant - M. Landau.

The computer program was used to check and analyze the planar electron gun design (gun no. 2) shown in Fig. A-3. Fig. B-1 shows the electron beam trajectories for the gun part which starts at the cathode and the beam forming (67.5° declined) electrode, and ends at the anode. The results of this computation were used as initial conditions for the computation and drawing of electron beam trajectories in the other parts of the gun. Fig. B-2 shows the focusing of parallel electron trajectories in the vicinity of the electrostatic lens (consistent of two electrodes at ground potential and a central electrode at -30 KV potential). It demonstrates the focusing effect of the lens.

The incorporation of this numerical tool in our research program enables us now not only to check various electron-optical designs and the effects of design modifications, but also to investigate sensitivity of the design to variations of various electrical as well as constructional parameters.

Vacuum Chamber

During the last year we have purchased and put into operation a Varian made U.H.V. system VT-114 to provide a chamber for the Cerenkov-Smith-Purcell

radiation experimental set up. The system is a standard 14" diameter U.H.V. pump which was adapted to our purpose with few minor modifications. It consists of two sorption pumps for rough pumping, 6 triode ionization pumps for high vacuum pumping, and a sublimation pump for pumping gas residues which are hard to ionize. We have found that a significant cost saving can be achieved by giving up the standard vacuum chamber and poppet valve and using the pump space (the "sump") for the experiment. All that was required was to order modification of four of the twelve standard $2\frac{3}{4}$ " ports of the system and substitute them by two 6" ports and two $4\frac{1}{2}$ " ports. A top view of the system is shown in Fig. 3. This approach has also an added advantage of reducing the pumping volume and area and thus reducing pumping time. There is though a possible disadvantage in getting this way the electron gun system closer to the static magnets of the ion pumps. This may produce a need to wrap parts of the electron beam path with magnetic shielding foils or build a degaussion coil.

With a baking option (which was not included in the present purchase but can be added) such a system can pump down to pressures of 10^{-10} Torr. This leaves us an option to use in the future high brightness field emission cathode filaments. However, at present we plan on using only LaB_6 cathodes in our electron guns. These cathodes can operate well without failure in pressure of 10^{-7} Torr which is routinely surpassed in our system, which is reaching the scale of 10^{-8} Torr inspite of the many O-rings used and without baking. The lack of vibrations during the operation of the ion pump-sorption pump system is a property which is of great advantage for our planned interaction experiments which require fine submicron adjustment between samples (gratings, dielectric slabs) and electron beam and optical beams.

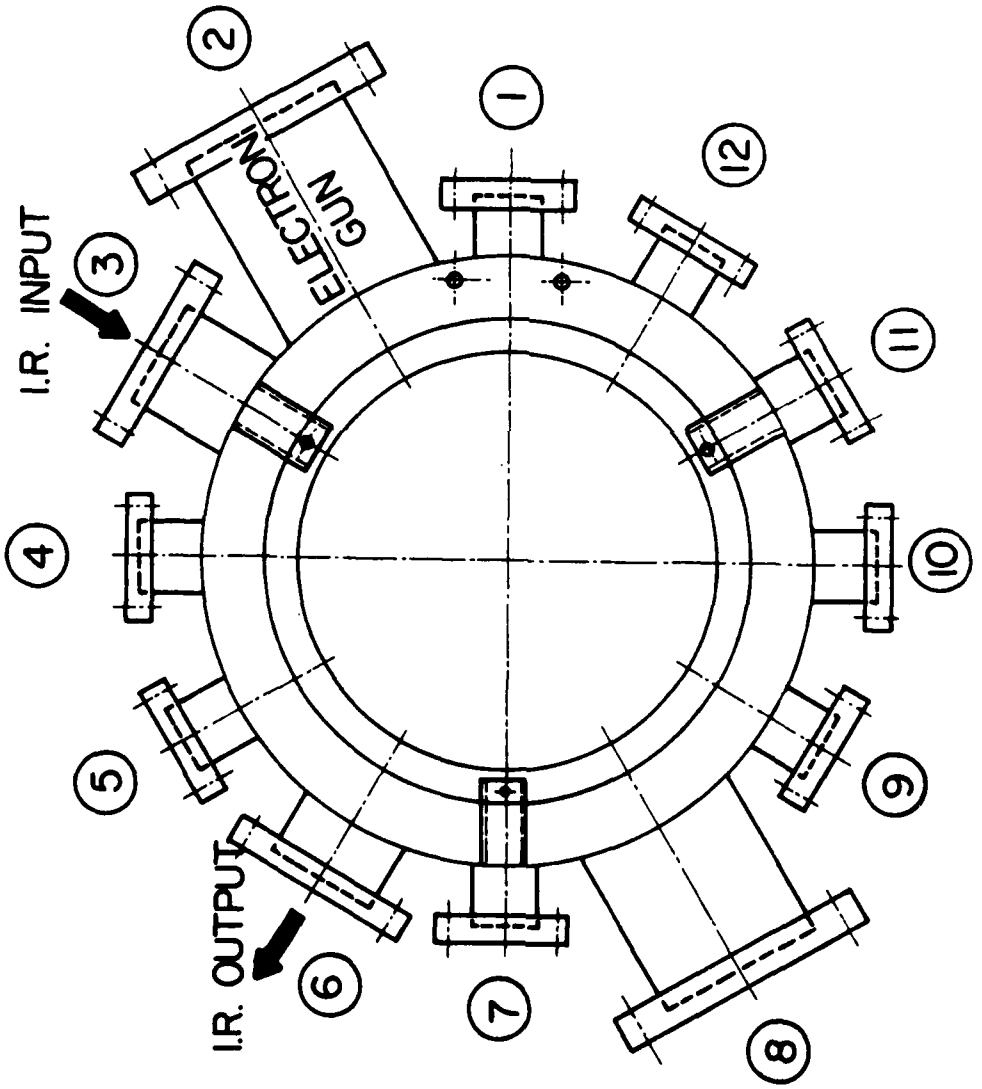

Fig. 3: The vacuum chamber.

To obtain the fine adjustment capability between the thin electron beam and the sample we have designed and constructed a sample manipulation system with the help of I. Levy, our consulting mechanical engineer. A photograph of this system is shown in Fig. 4. The system consists of three linear Viton feedthroughs (the three vertical poles which are pushed separately by three fine differential micrometers (Physik Inst. P-128). These micrometers make 50 μ per turn, read 1 μ per division and have traversal length of 15 mm (with the coarse adjustment). The micrometers are turned slowly at a rate of 1 turns/min. by three synchronous electrical motors with reversible sense of rotation which are controlled from a control box. By operating all three motors at the same time we can get accurate vertical motion of the sample (to be attached to the three polls). The sample will move at a conveniently controllable rate of 50 μ/minute. The operating of only one or two motor out of the three allowstwo tilt degrees of freedom for aligning the sample with the electron beam.

Other parts and accessories like various electrical and mechanical feedthroughs and optical windows has been orders or are constructed.

High Voltage Power Supply

A high voltage (-70 KV) power supply for operating in the experimental set up (Fig. 1) was purchased from Universal Voltronics. The power supply, BRE70-8, has the following properties:

Voltage range: 0-70 KV

Current range: 0-8 mA

Ripple : 10^{-4}

Stability : $(2\text{-}5) \times 10^{-4}$

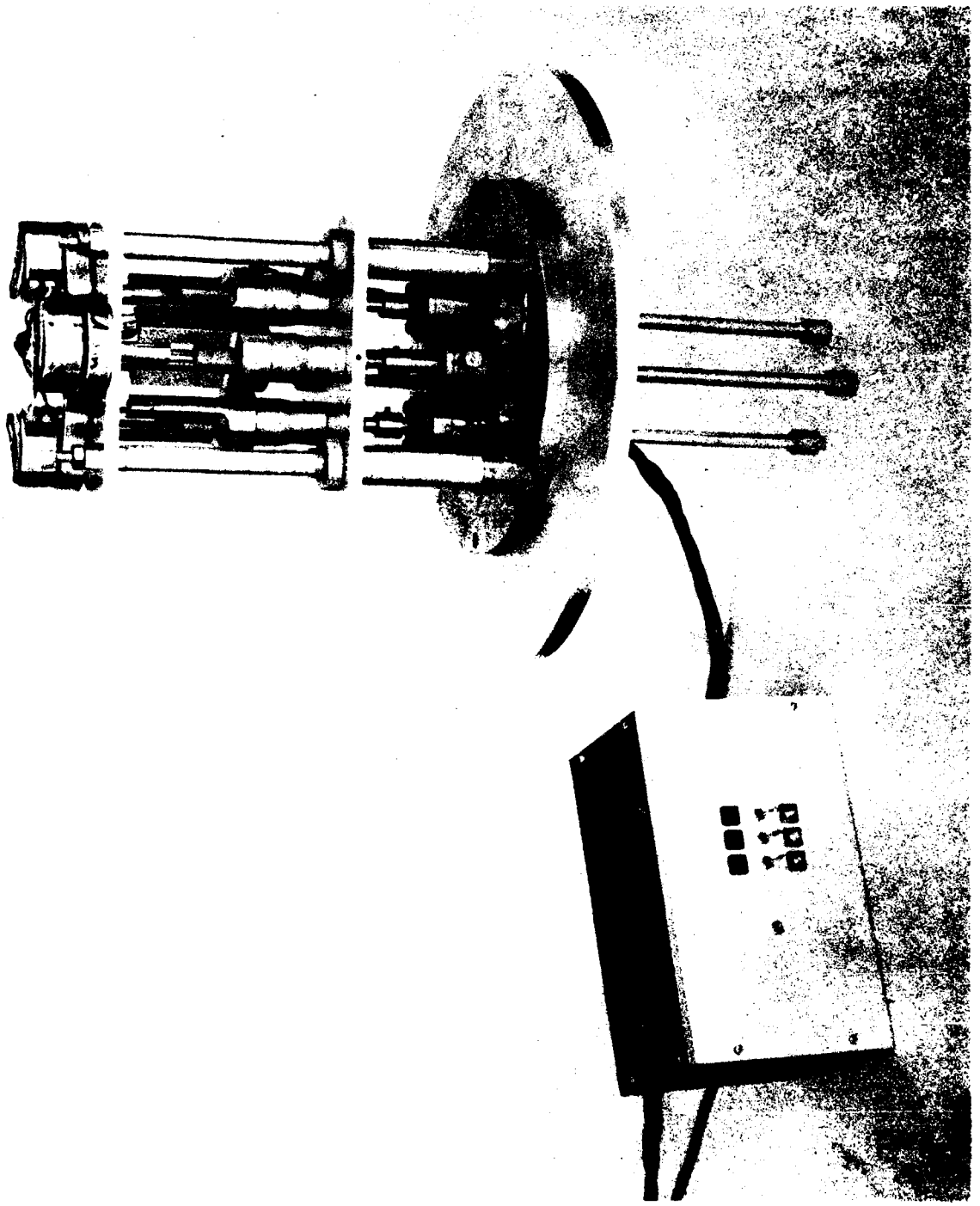

Fig. 4: Sample manipulation system and control box.

In addition we have ordered a precision monitoring option for accurate voltage measurement and a fillament heating option. The fillament heating option will provide 10 V 10 A AC heating current for heating the cathode which should be floated over the high voltage (-70 KV). Thus in contrast to the scheme of Fig. 1 we will not use the isolation transformer for supplying cathode heating power as long as power requirement will be met by the fillament heating option of the power supply.

The long delivery time originally quoted and in addition delays due to the adding of the fillament heating option and other manufacturer's delays, has held up the arrival of the H.V. Power supply for a rather prolonged time, and is causing certain delays in the farther development of the experimental set up and in starting planned experiments. The manufacturer has recently promised to deliver the equipment on March 1980.

Other high voltage equipment like cables and terminals has been ordered but completion of the rest of the electronic system and testing of various high voltage components and systems like H.V. feedthroughs, terminals, voltage deviders will have to await the arrival of the power supply.

Electron Gun Construction and Experiments

The planar electron gun design (gun no. 2) has been reduced into machine shop drawings by Eng. I. Levy, who consults us on mechanical design. It was handed over to our mechanical shop for precision machining and construction. The electron gun electrodes are designed to be mounted on three accurately parallel ceramic rods, which are mounted on one of the vacuum chamber 6" flunges. The high voltage feedthrough is mounted on the same flunge (port no. 2 in Fig. 3). The ceramic rods and the high voltage feedthroughs have

been special order manufactured for us and are already mounted on a 6" conflat flange blank (photograph in Fig. 5). The basic mechanical design of gun no. 2 is shown in Fig. A-11.

Directly heated wedge shaped single crystal LaB_6 cathodes have been special ordered from Kimball-Physics to be used in gun no. 2. A photomicrograph of one of these cathodes is shown in Fig. 6. The 0.5 mm × 0.5 mm LaB_6 block is mounted on a thin flexible graphite strip which provides direct electrical heating of the tip and a chemically passive mechanical support. Some of the cathodes were ordered with flattened tip of 25 μ × 500 μ rectangular shape.As discussed in App. A,this rectangular face is designed to be imaged by the electron gun optics and produce a ribon shapped beam of 10 μ × 500 μ cross section dimensions at the focus, and depth of focus of 2-10 cm.

The development work of gun no. 2 is still pursued in the machine shop. Due to the tight tolerances and the difficult planar shapes, it turned out to be a harder task than earlier anticipated. The main parts which delay now the completion of the gun is the cathode assembly and alignment system and the grid and slit systems.

As an intermediate step, which could allow preliminary evaluation of the cathodes, and will permit preliminary Smith-Purcell experiments at moderate energies (20-35 KV) and longer wavelengths, we decided to construct in the meanwhile two versions of a simpler gun which were designed and constructed at a relatively short time:

Gun no. 1: This gun (whose mechanical design is shown in Fig. A-12 and its photograph shown in Fig. 5) is basically a simple triode gun which includes only a cathode, a grid electrode and a punctured anode, and has no

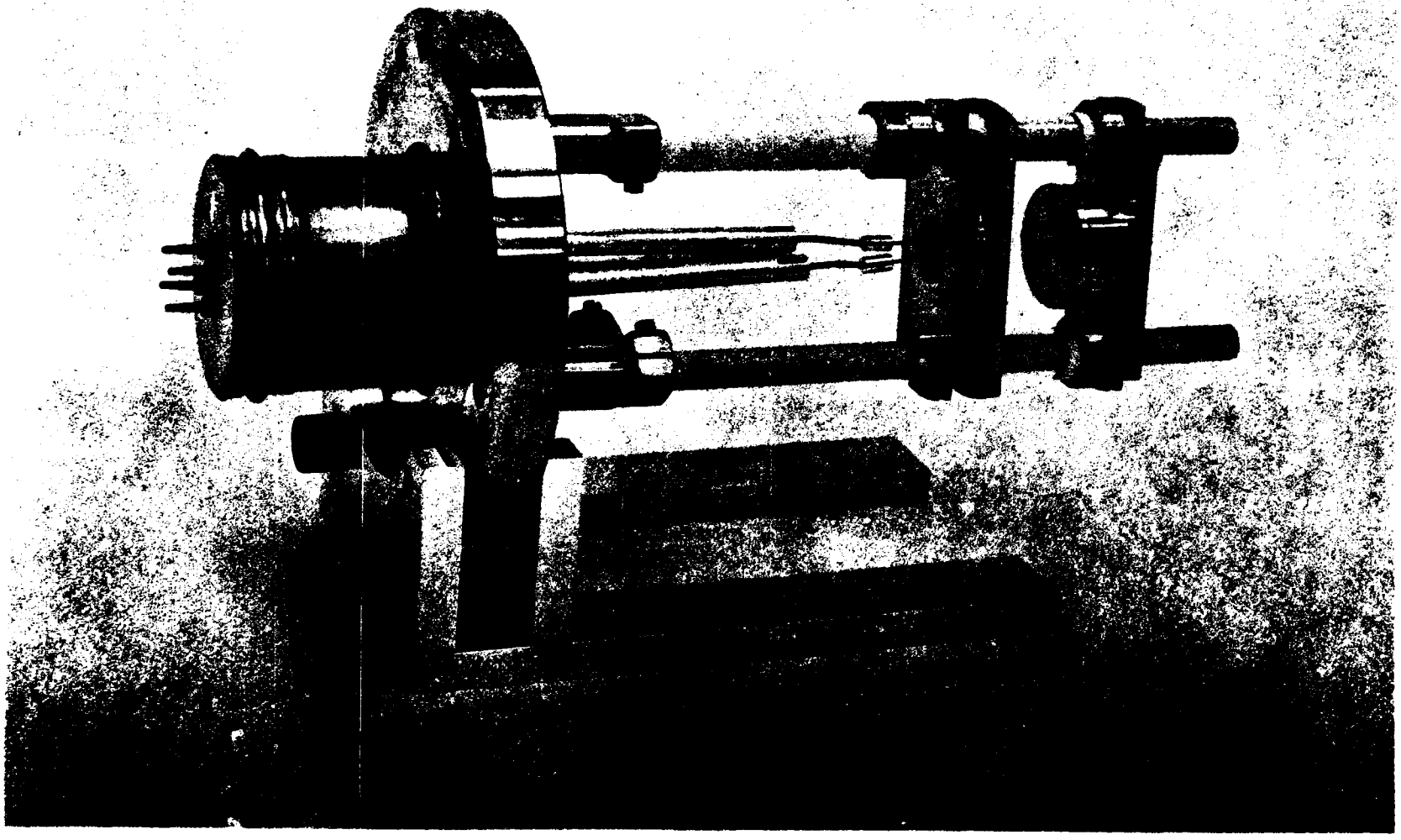

Fig. 5: The electron gun - H.V. feedthrough assembly sitting on a stand. The electrodes which are mounted on the ceramic rods are those of electron gun no. 1A.

Fig. 6: Microphotography of the tip of a wedge shaped LaB_6 cathode. The crystal is attached to a graphite strip. The wedge tip length is 0.5mm.

focusing means. The gun is made with cylindrical symmetry, and produces a pencil shaped beam of about 1 mm diameter.

Gun no. 1A: This gun which is being constructed now is an improved version of gun no. 1 and includes in addition to the electrodes of the first version also a conically shaped beam focusing electrode (with 67.5° half opening angle) to form a Pierce gun structure. We intend to use this gun for preliminary Smith-Purcell experiments at electron energies 20-35 KV and long wavelengths (up to λ = 1 mm).

Figs. 7-9 are the results of recent experiments with gun no. 1 intended mostly for evaluating the Kimball cathode characteristics. Fig. 7 displays the cathode current as a function of cathode heating power. We see that 7-8 Watt should be enough to heat our cathode. Fig. 8 displays the I-V characteristics between the cathode and grid electrodes for 8.25 Watt heating power. The curve starts tapering around I_c = 50 mA where temperature controlled electron emission starts. Bellow 30 mA the current behaviour seems to be space charge controlled. Fig. 9 shows the triode I-V characteristics for two grid voltage values.

Optical Experiments

In the longitudinal interaction free electron lasers (which includes Cerenkov-Smith-Purcell and longitudinal electrostatic bremsstrahlung FELs) the interaction of the electron beam with the electromagnetic wave is carried out via the longitudinal electric field component of a TM electromagnetic mode. To get a large longitudinal field and strong interaction, a

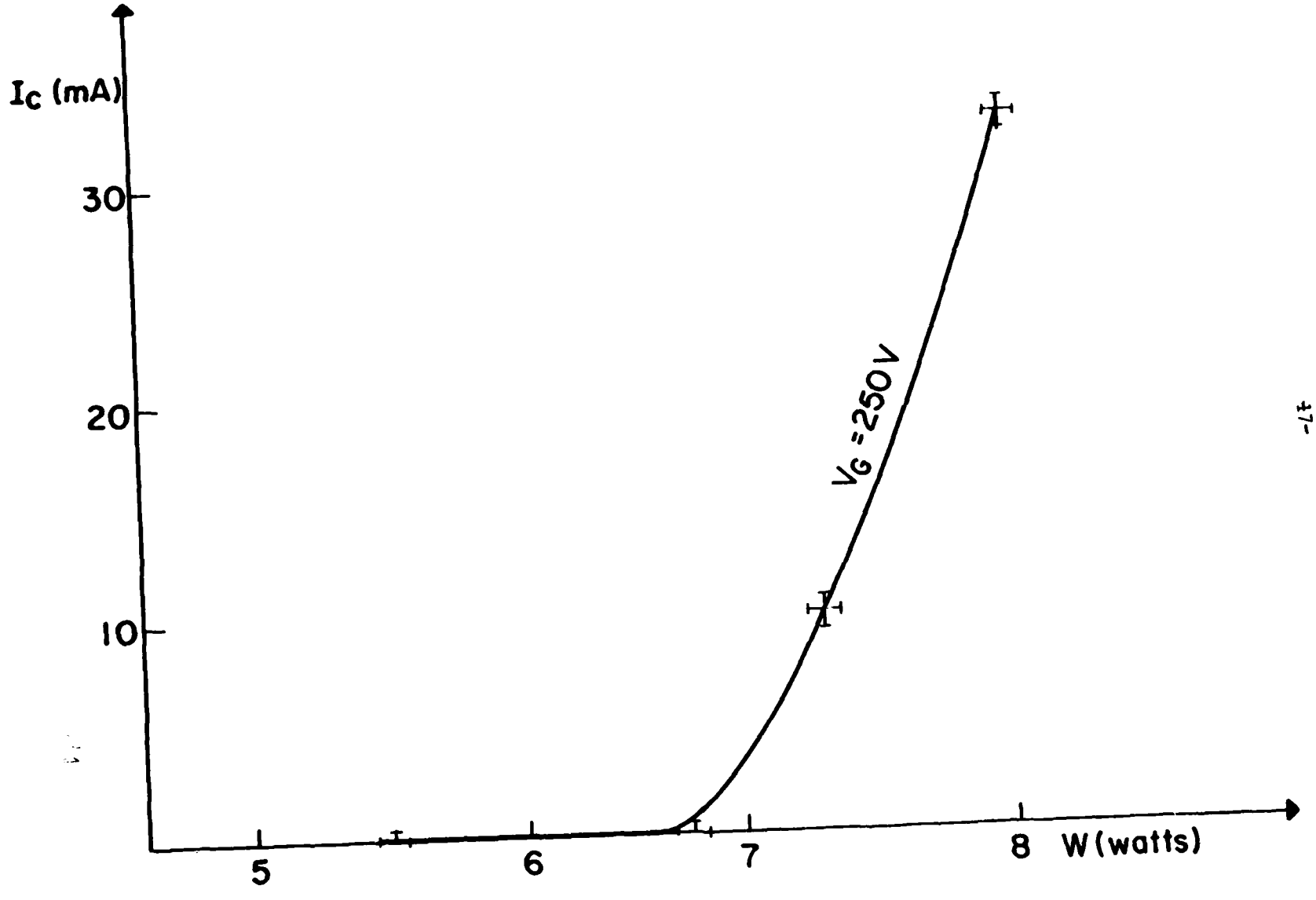

Fig. 7: E-gun no. 1 cathode current vs. filament heating power.

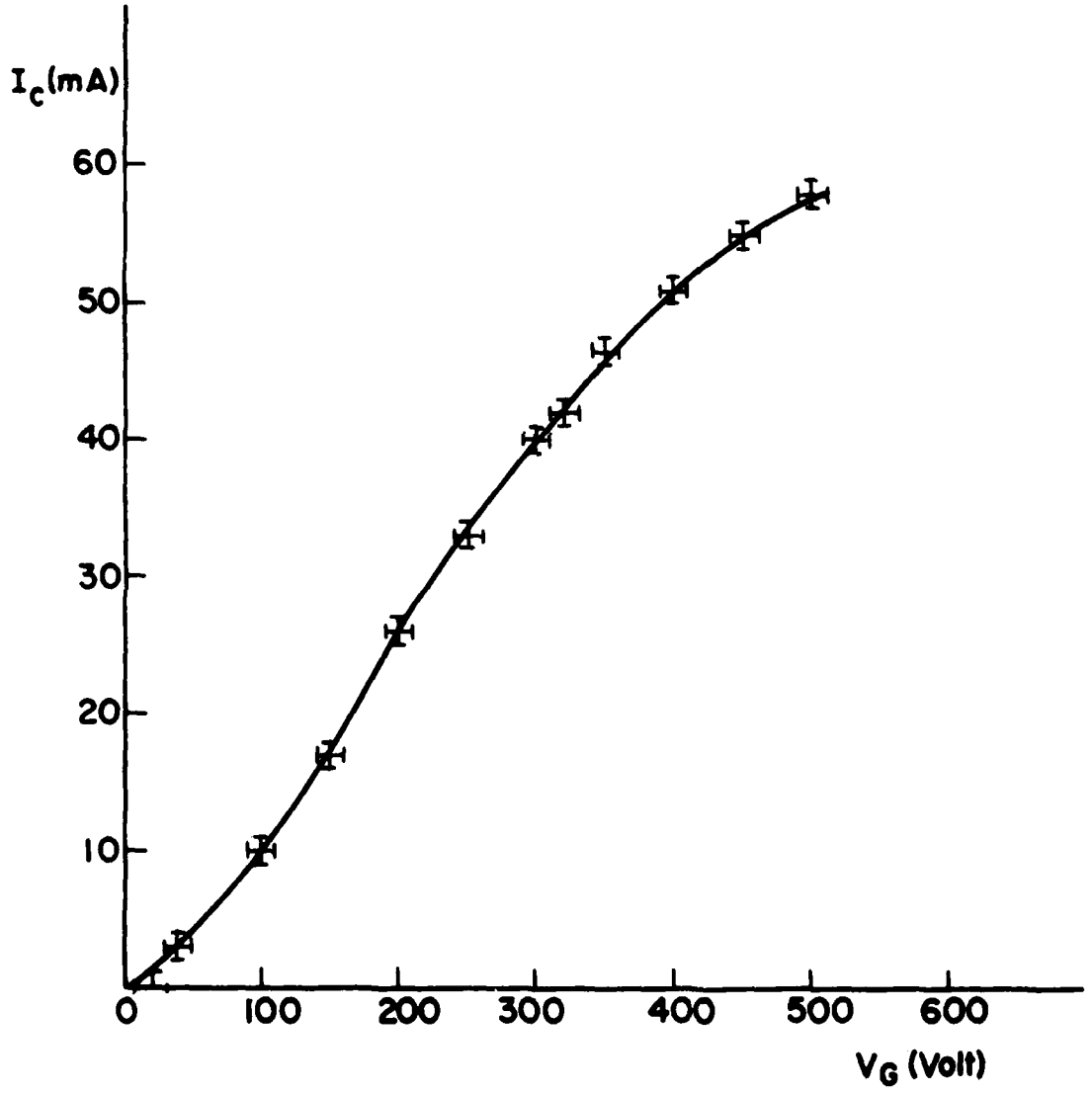

Fig. 8: E-gun no. 1 cathode current vs. grid voltage characteristics. Cathode heating current is 0.25 Watt. Anode is open circuited.

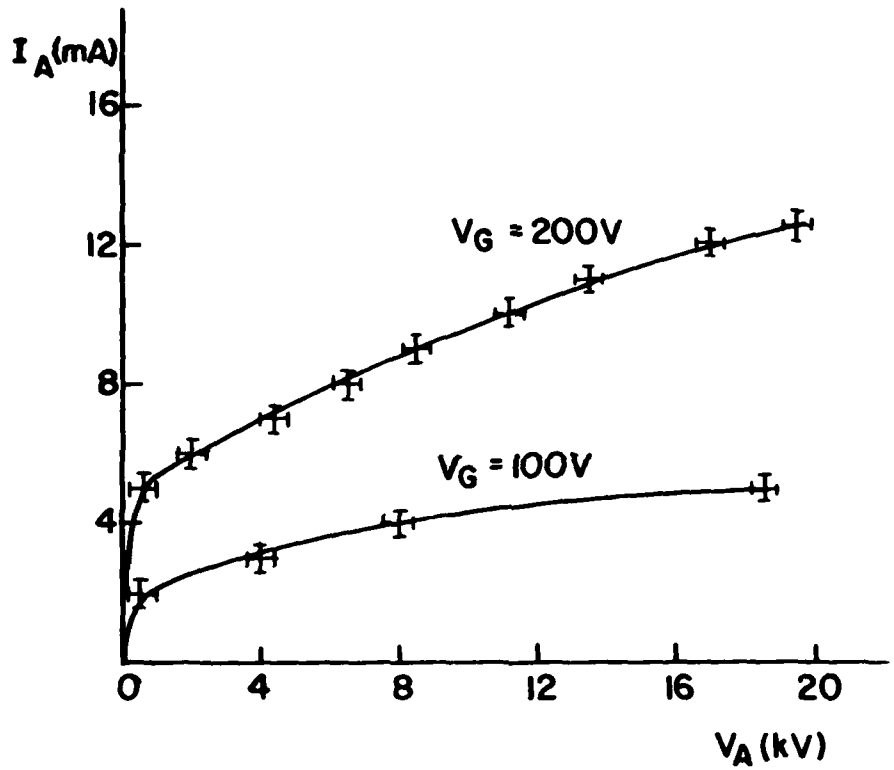

Fig. 9: E-gun no. 1 I-V characteristics of anode current vs. anode voltage for two values of grid voltage. Cathode heating current is 8.25 Watt.

high order TM mode should be used. However, high order TM optical modes usually suffer appreciable attenuation in metalic waveguide structures. To get net amplification in a laser amplifier structure or to satisfy an oscillation condition in a laser oscillator structure, it is of course necessary that the laser gain available will overcome the passive waveguide losses.

In order to evaluate the waveguide losses of various waveguiding structures at 10.6 μ and find ways to minimize them, we have carried out in the last two years experiments on reflection losses and waveguiding of CO_2 laser light in various materials and structures. Some of this experiments were reported in our first year progress report (dated Feb. 28, 1979). Some more experimental work which was carried out last year with polarized laser light is reported in Appendix C of the present report.

In particular we have examined in further detail wave propagation in waveguide structures with large cross-section aspect ratio. These structures (Fig. C-1) were suggested in the first report as advantageous structures for use in longitudinal interaction FELs for the reason that they allow relatively low loss propagation of electromagnetic modes with an appreciable longitudinal electric field component. The interacting mode should be one which has a low order mode number (small "zig-zag angle") in the dimension of the narrow waveguide walls, and high order mode number (large "zig-zag angle") in the dimension of the wide waveguide walls. Due to the high "zig-zag angle" in the wide dimension the mode has a large longitudinal field component. Inspite of the high "zig-zag angle" in this dimension the losses due to absorption in the narrow walls is small because

there are only few "reflections" in the wide dimensions. There is also little absorption in the wide walls because the mode order number (or "zig-zag angle") in the narrow dimension is small. Thus this structure will be most appropriate for a longitudinal FEL structure which utilizes a ribbon shaped electron beam (to provide high "filling factor" for the laser gain).

Measured transmission curves at 10.6 μ wavelength of large aspect ratio waveguides composed of stainless steel and polished glass walls are shown in Figs. C-6 to C-10. Further details are explained in the appendix.

Distributed Feedback Free Electron Lasers

It occured to us that the concept of DFB - distributed feedback (feedback due to Bragg reflection from a periodic structure placed within the laser active region)[10] can be adapted to free electron lasers with certain advantages. Perhaps, the advantage of DFB is most significant when the free electron laser is based on pulsed intense relativistic electron guns which usually have very short pulse duration (few tens of nano-seconds). For such FELs the pulse duration is too short to sustain laser oscillation in a conventional Fabri-Perot resonator structure, this is because there will be only few traversals of the electromagnetic wave across the resonator structure before the electron beam pulse terminates. When the feedback mechanism is provided right in the active region, this problem is solved.

II. Program Progress and Conclusions

During the first two years of research sponsored under grant 77-3445 a research effort was developed with the aim to increase understanding and prepare for experiments on electron beam interactions with electromagnetic waves and particularly free electron lasers. Presently the research is conducted by two investigators: A. Gover and S. Goldsmith and two research assistants (graduate students): P. Dvorkis and M. Landau. Collaborative research relation have been developed with a number of research groups active in the same field: P. Sprangle and V. Granatstein of N.R.L., P. Schlesinger and T. Marshall of Columbia University, and Y. Carmel and his research group in Israel Ministry of Defense R & D Agency.

The theoretical research that has been conducted under the grant focused mostly on Cerenkov-Smith-Purcell FELs.[11-14] However we have shown that the different kinds of FELs which are now under consideration are closely related, and developed comprehensive unified models for all of them.[11,12,15] Analytical work was done on the more familiar magnetic bremsstrahlung FEL[3] as well as on new FEL schemes.[1,2]

Significant development effort has been devoted to the establishment of a new laboratory facility for conducting free electron laser experiments at low energy. This includes technological means and design capabilities in a number of broad fields like infra-red optics, high vacuum systems and electron optics. The first year of research under the present program was devoted mostly to analytical work. This served to supply a basis for

designing the planned experiments, defining and calculating their parameter. On the experimental part, progress has been made in the first year mostly on the optical part of the experiment, establishing generation and detection capabilities in the infrared (10.6 μ), and conducting preliminary waveguiding experiments in passive structures. Progress in the establishment of the experimental setup has been made in the second year during which a high vacuum system VT-114 was purchased and put into operation. Other high vacuum parts like electrical and mechanical feedthroughs and optical windows were purchased and fabricated, and a sample manipulation system was built. A high voltage (-70 KV) power supply was purchased but has not arrived yet todate. Important progress was made in establishing design and technological capabilities of electron optics, including the operation of a computer program for calculation of electron trajectories, the design, fabrication and testing of electron gun no. 1 and its cathodes, and the completion of electronic and mechanical design of electron gun no. 2.

According to our plan the third year of research should be devoted to the completion of the construction of the experimental set-up for running spontaneous Cerenkov-Smith-Purcell experiments, and preparing for stimulated emission experiments. However prolonged delays in delivery of some major orders will cause certain delays in the planned schedule and will require alternative approaches. Most major delay has been in the delivery of the high voltage power supply, which has been long delayed and according to the manufacturer's latest promise should arrive only this month. There has been a long delay also in the fabrication of electron gun no. 2 which turned out

to be a mechanical design and machining task more difficult than first anticipated, and is still under work in our machine shop. Consequently we expect now that the completion of the construction of the experimental system based on the fine beam gun no. 2 will be completed only in the end of this year and experiments with it can be executed only in a fourth research year.

Concurrently with the continued work on gun no. 2 and the electronic system based on the 70 KV power supply, we plane to work during the third year also on an alternative approach based on gun no. 1A and lower voltages (20-35 KV) which is expected to produce preliminary experimental results of electromagnetic radiation from electron beam already during the third year. However, due to the fact that this electron beam is much coarser than gun no. 2 and the acceleration voltage is lower, the experiments will have to be carried out at longer wavelengths (submillimeter wavelengths). In addition, some of the Smith-Purcell experiments planned, will be carried out in collaboration with Y. Carmel using an existent intense relativistic electron gun system[16,17] which is prepared for experimentation during this year.

III. Scientific Publications and Presentations

The following papers were published during the reporting period or are being prepared for publication:

1. A. Gover "A Free Electron Laser Based on Periodic Longitudinal Electrostatic Bremsstrahlung". To be published in Physics of Quantum Electronics, Vol. 7, S. Jacobs, M. Sargent and M.O. Scully (Eds.), Addison Wessley (1980).
2. A. Gover "An Analysis of Stimulated Longitudinal Electrostatic Bremsstrahlung in a Free Electron Laser Structure". Submitted for publication.
3. A. Gover and P. Sprangle "'Exact' Gain Expression for the Free Electron Laser and Effects of Transverse Velocity Spread and Incoherence of the Pump". Submitted for publication.
4. A. Gover and P. Sprangle "The Operating Parameters of Magnetic Bremsstrahlung, Electrostatic Bremsstrahlung, Cerenkov-Smith-Purcell and Compton-Raman Free Electron Lasers". In preparation.

In the following occasions during the reporting period the research done under the present grant was reported,and the grantor was acknowledged:

(1) ONR Workshop on Free Electron Generators of Coherent Radiation, Telluride, Colorado, Aug. 13-17, 1979.

(2) Seminar in National Science Foundation, Washington D.C., Summer 1979.

(3) M.I.T. National Magnet Lab. and Lincoln Lab., Boston, Massachussets, Summer 1979.

(4) 11th Convention of IEEE, Israel Section, Oct. 23, 1979.

APPENDIX A: A thin sheet beam electron gun design - Kurt Amboss

Introduction

The free electron laser experiment utilises a sheet electron beam. In the initial calculations the beam dimensions in the interaction region were assumed to be 10 cm long in the direction of electron flow, 10 micron thick and 100 micron wide and the spacing from the grating was taken to be 5 micron. The beam voltage was assumed to be in the order of 30 ~ 70 Kv. and the current density 0.1 A/cm^2. In designing the experimental equipment we have attempted to provide not only this beam, but also a flexible environment which would allow the beam characteristics to be changed between wide limits. As a result the electron gun is designed as part of an optical bench which allows interelectrode spacings to be changed with relative ease. This is done by mounting all electrodes on ceramic rods using ceramic tubes as spacers.

Achievement of the above beam parameters is not a trivial problem, in particular when the experimental circumstances require a system which can be let down to air at will. In view of this the electron gun design uses a Lanthanum Hexaboride (LaB_6) cathode which has shown itself to be an excellent material for use in demountable system. A field emission cathode was contemplated but was rejected on account of the stringent vacuum requirements required for it's operation.

The design of the sheet beam

A fundamental limit to the attainable current density j_i in a beam is set by the Langmuir limit which relates j_i to the emission density j_c of the cathode, the cathode temperature T, the beam voltage Φ_A and the limiting angle θ_i of figure 1 with which the electron trajectories can converge onto a point P in the beam under consideration. For sheet beams the Langmuir limit is

$$j_i = j_c \frac{2}{\pi^{1/2}} \left(\frac{e\Phi_A}{k\,T} \right)^{1/2} \sin\theta_i \qquad (1)$$

Figure 2 shows the limiting value of θ_i in the experimental set up to be 5×10^{-5} radian. LaB_6 requires an operating temperature of about $1750^{o}K$ for an emission density of $6A/cm^2$ which may be taken as a conservative upper limit for repeatable demountable operation. With these values used in the Langmuir limit a beam voltage of 30 kv permits a current density of $j_i = 0.15\ A/cm^2$ in the beam to be obtained. In practice the theoretical limit is degraded by about a factor of 2 at best and for this reason an operating voltage of 65 kv was chosen to give $j_i = .22\ A/cm^2$. Other benefits are derived by operating at high voltage; the grating dimensions are increased and the beam is also "stiffer" and thus less sensitive to perturbing fields. The disadvantages of high voltage operation are of course the increased cost of equipment and the need to subject the design to voltage breakdown criteria.

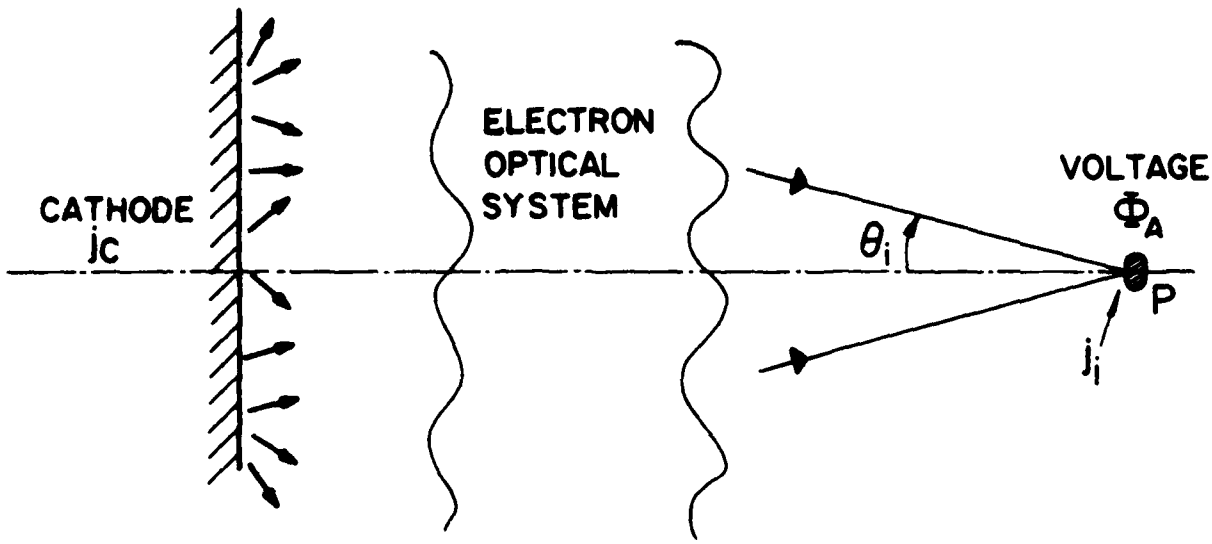

FIG. A-1
THE PARAMETERS OF THE LANGMUIR LIMIT

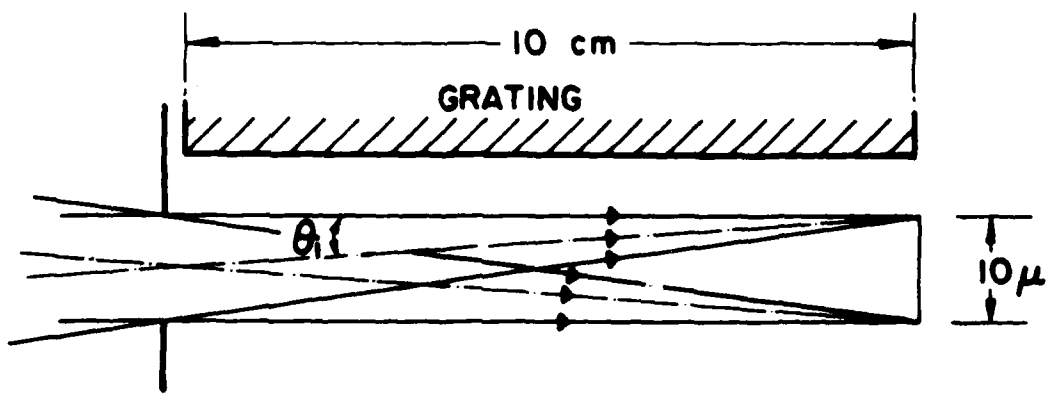

FIG. A-2
THE LIMITING VALUE OF θ_i IN THE EXPERIMENT

Our electron gun design is shown schematically in figure 3. A parallel flow of electrons of uniform current density is produced by a planar, aperture gridded Pierce gun. However the fringing field of the hole in the anode diverges the sheet beam and a unipotential lens is used therefore to reconverge the beam and to produce a 10 micron high image of the cathode near the downstream end of the grating. A rectangular 10 micron high aperture immediately behind this lens trims the beam to the correct dimension at the beginning of the grating.

The design of the Pierce gun is based on the space charge limited flow between two parallel infinite planar electrodes. If these are spaced a distance d apart and if Φ is the voltage on the anode, the space charge limited current density j_c drawn from the cathode is

$$j_c = 2.33 \times 10^{-6} \Phi_A^{3/2}/d^2 \quad . \tag{2}$$

For $j_c = 6A/cm^2$ and $\Phi_A = 65$ kv the diode spacing is

$$d = 2.54 \text{ cm} \tag{3}$$

Inspite of the high operating voltage thermal velocity effect play a major role in determining the electron optics. The characteristics of the beam are, to first order, explainable in terms of the motion of two trajectories: one which we label as R_e and which starts from the edge of the cathode with zero transverse velocity, and the other labelled σ which starts from the cathode, on axis, with transverse velocity $\sqrt{kT/m}$.

Fig. A-3: The design of e-gun no.

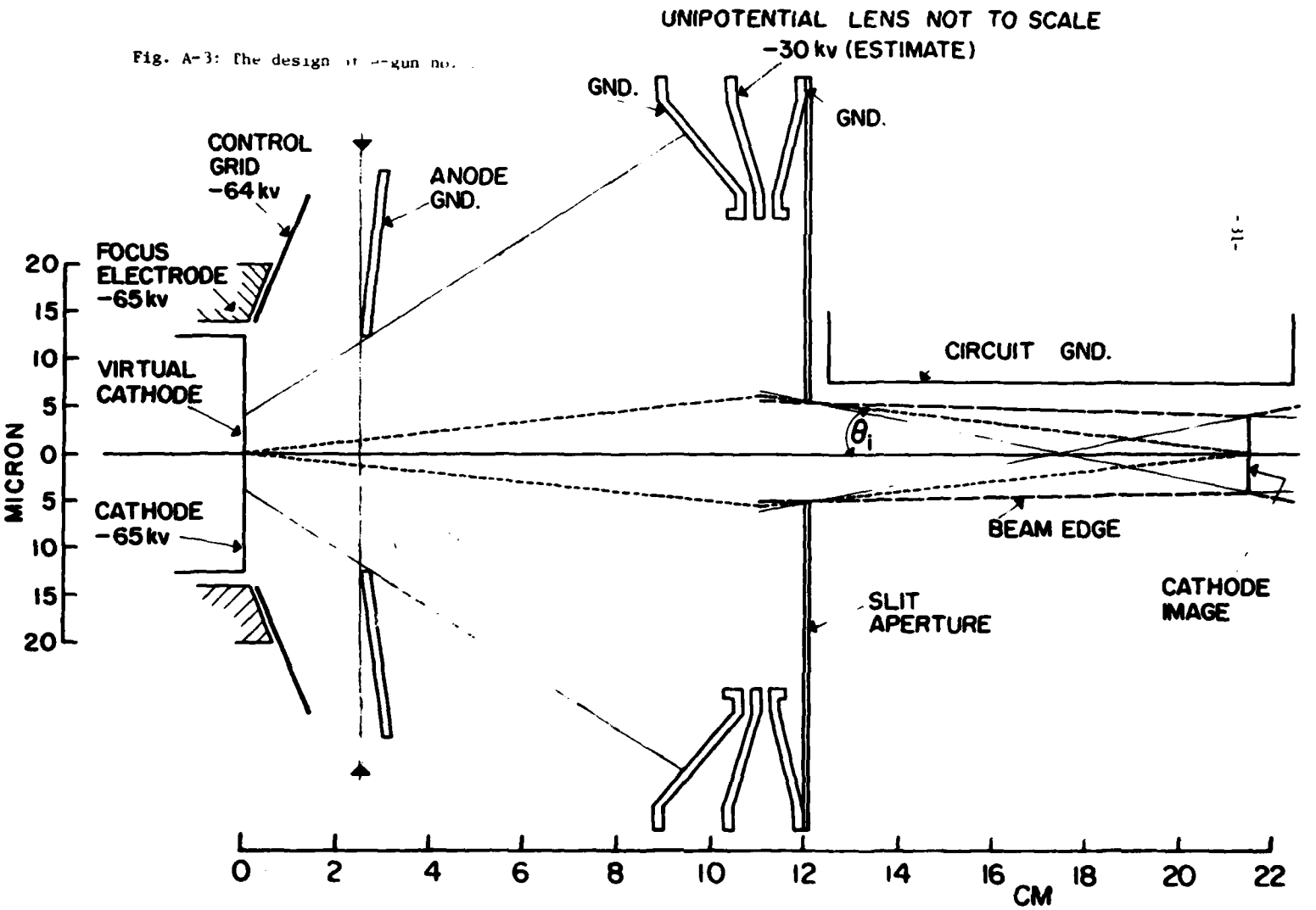

Their paths in the Pierce gun are shown in figure 4, and are readily calculated by assuming that the dispersion of the beam leaves the axial potential distribution unaltered. It is also assumed that the effect of the anode aperture slit can be described by a thin divergent cylinder lens in the plane of the anode.

The electron optics of the diode

The electron optics of the planar diode can be seen from figure 4. The electric field of the diode produces a virtual cathode which becomes the object of the anode lens. The latter, being a divergent lens, produces an upright virtual, demagnified image of the cathode which we show coincides with the cathode.

Consider the σ electron; at any z location $\sigma' = d\sigma/dz$ is given by

$$\sigma' = \frac{v_{TH}}{\sqrt{2\eta\Phi}} = \sqrt{\frac{kT}{e\Phi}} \qquad (1)$$

$\sigma'_A = 1.5\times10^{-3}$ at the anode, before entering the anode lens. Also

$$\sigma = v_{TH}\, t$$

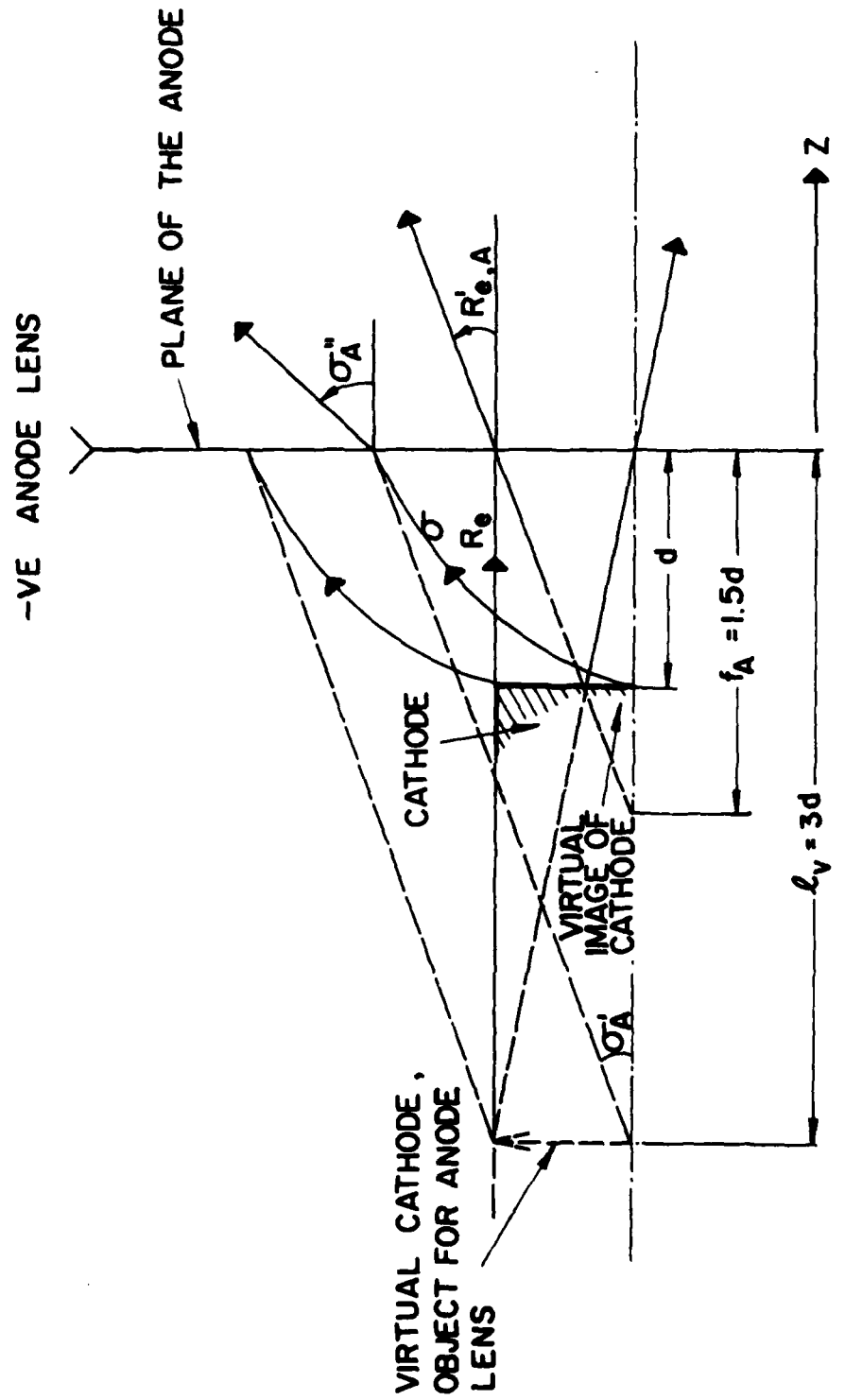

FIG. A-4 THE ELECTRON OPTICS OF THE APERTURED PLANAR DIODE.

where t is the transit time to position z from the cathode. But since

$$dz = \sqrt{2\eta\Phi}\, dt = \sqrt{2\eta\Phi_A}\, (\frac{z}{d})^{2/3}, \tag{5}$$

we find that

$$\sigma = 3d \sqrt{\frac{kT}{e\Phi_A}} (\frac{z}{d})^{1/3} \tag{6}$$

At the anode, where $z = d$ $\sigma_A = 114 \times 10^{-4}$ cm. The position ℓ_v of the virtual cathode, which forms the object for the anode lens is given by

$$\ell_v = \sigma_A/\sigma'_A = 3d \tag{7}$$

It is evident by inspection of figure 4, that since Ru is constant in the Pierce diode that the height of the virtual cathode is the same as the cathode. This virtual cathode serves as the object for the anode lens.

The Davisson-Calbick formula for the focal length f of an aperture lens is

$$\frac{1}{f} = \frac{E_1 - E_2}{2\Phi_A} \tag{8}$$

where E_1 and E_2 are, respectively the electric fields on the upstream and downstream sides of the aperture. In the Pierce gun $E_2 = 0$ and

$$E_1 = -\frac{4}{3} Kd^{1}/3 \qquad (9)$$

since $\Phi = Kz^{4}/3$, where K is a constant. At the anode, where $z = d$ $\Phi_A = Kd^{4}/3$ so that

$$\frac{1}{f} = -\frac{2}{3} d = -\frac{1}{3.81} \text{ cm}^{-1} \qquad (10)$$

If ℓ' is the location of the image formed by the virtual cathode at ℓ_v then from the lens formula

$$\frac{1}{\ell'} + \frac{1}{\ell_v} = \frac{1}{f} \qquad (11)$$

we find that $\ell' = -d$ that the image coincides with the location of the cathode and is demagnified by a factor of 3.

Choice of the object to be imaged.

There are two approaches to producing the beam parameters in the interaction region. The first consists in using the demagnified virtual image of the cathode as a virtual object and to produce a real image of it near the downstream end of the grating by means of the unipotential lens. The other approach is to flood a slit aperture located immediately behind the anode with electrons and to use it as a real object which is again imaged in the same location.

We consider the latter alternative first. Figure 5 shows the result of calculations by Crunly of the dispersion of a sheet beam by thermal electrons. The figure shows for $Ru/\sigma < 1.5$ that the current density on the axis is reduced by the migration of the thermal electrons below the value at the emitter. If the intensity at the flooded object aperture is to equal the value at the cathode Ru must be approximately equal to $1.5\ \sigma_A$. Hence the width of the cathode is approximately $2R_e = 3\sigma_A = 3.42 \times 10^{-2}$ cm. It is necessary to start with a relatively long cathode since there is no focusing in the plane of the circuit. Assuming a length of cathode of about 3mm leads to an emitter area of 6.48×10^{-3} cm^2 and with cathode loading of $6A/cm^2$, to a cathode current of about 38 mA.

The other alternative, imaging the virtual cathode at unit magnification, involves the use of considerably less emitter current; the penalty however is the fabrication and alignment of a very narrow cathode in the focus electrodes. Since the virtual cathode has a width of 10 micron at unit magnification the real cathode is 30 micron wide and the emitter area, for a cathode which is 2mm long also is $6 \times 10^{-4} cm^2$ and the cathode current is 3.6 mA.

In this approach which we pursue the only aperture is that shown in fig.3 immediately beyond the imaging lens. [In a sense we may regard the system to have another aperture at the cathode.] To calculate the beam parameters at the defining aperture we require the values of R_e and σ in the location of the slit aperture. The dimensions given in fig.3 are used.

The region beyond the anode

We assume the electron flow beyond the anode to be in field free space since the beam has a value of $R_e/\sigma = .13$ at the anode and is quite dispersed so that space change forces may be neglected. Beyond the anode lens the σ electron drifts with a slope σ_A'' as illustrated in figure 4. Using equation 11 we find that

$$\sigma_A'' + \sigma_A' = \sigma_A/f \tag{12}$$

which on using the values calculated previously gives $\sigma_A'' = 4.5\text{x}10^{-3}$. The path of the σ electron is therefore

$$\sigma = \sigma_A + \sigma_A'' (z-z_A) \tag{13}$$

where z_A is the z location of the anode. At the center of the unipotential lens $z = 11$cm the value of σ is found to be $495\text{x}10^{-4}$ cm.

The calculation for R_e at the center of the lens is made in identical fashion. The R_e electron has a slope $R'_{e,A}$ immediately after the lens which is given by

$$R'_{e,A} = R_{e,A}/f \tag{14}$$

which is found to be $R'_{e,A} = 3.93\text{x}10^{-4}$. As the path of the R_e electron is

$$R_e = R_{e,A} + R'_{e,A}(z-z_A) \tag{15}$$

the value of R_e at the center of the unipotential lens is therefore $R_e = 48\text{x}10^{-4}$ cm. The value of R_e/σ at the focusing lens is therefore 0.097.

A rough check of the current density at the aperture may be obtained from the theory of Crumly. His equation 3.31 may be written as

$$j = \frac{1}{\sqrt{2\pi}}\, j_c \left(\frac{R_{e,c}}{R_e}\right) \int_{y-R_e}^{y+R_e} \exp - y^2/2\sigma^2 \, d\left(\frac{y}{\sigma}\right) \tag{16}$$

where $R_{e,c}$ is the halfwidth of the emitter and y the transverse displacement of the point of observation from the axis of symmetry. For y corresponding to the half-width of the slit y/σ is small, and the exponential term in (16) may be expanded as a power series in y/σ.

Thus

$$j = j_c \left(\frac{R_{e,c}}{R_e}\right) \int_{y-R_e}^{y+R_e} (1-\frac{y^2}{2\sigma 2} + \ldots)\, d(\frac{y}{\sigma}) \qquad (17)$$

and

$$j = \frac{2 j_c R_{e,c}}{\sqrt{2\pi}\ \sigma} \qquad (18)$$

By similar triangles $\sigma = 445 \times 10^{-4}$ cm at the slit. Hence the calculated current density at the slit is 0.16 A/cm^2, a value which is in fair agreement with the value of 0.22 A/cm^2 calculated from the Langmuir limit

The length of the cathode

It is desirable to maintain a uniform current density distribution also over the width of the beam. No focusing is provided in this direction and the beam gradually disperses. If we wish to obtain a uniform distribution in the trimming aperture which we will assume may vary from 100 micron to 500 micron in length then as the dispersion curve, fig5, shows the value of R_e/σ must be at least $Re/\sigma = 2.0$. Here we have adopted the subscript to denote the values in the unfocused direction. Up to the anode σ is identical with σ; however since there is no lens

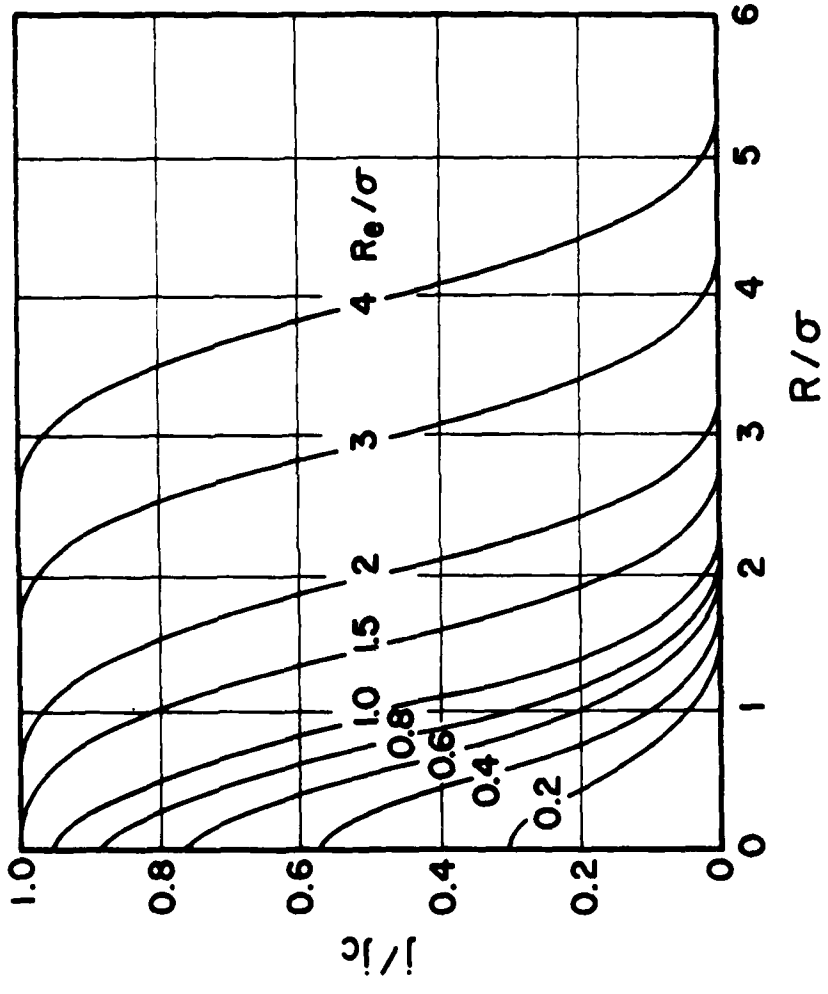

FIG. A5
DISPERSION OF A THERMAL SHEET BEAM

action in this direction $\sigma''_{,A} = \sigma'_{,A} = 1.50\text{x}10^{-3}$. The beam drifts for about 20 cm beyond the anode and therefore at the end of the circuit $\sigma = 114\text{x}10^{-4} + 1.50\text{x}10^{-3}\text{x}20 = 414\text{x}10^{-4}$cm. The corresponding value of $R_e = 2\sigma$ is therefore 0.8 mm and the length of cathode required is about 2 mm with an allowance for end effects.

Efficiency of the gun

A cathode 2mm long and 30 micron high, emitting with a current density j_c of $6A/cm^2$ will result in a cathode current of 3.6 mA. The current through the defining slit, 5 micron high and 500 micron long, with current density $j = 0.17\ A/cm^2$ amounts to 4.25 microamps. The efficiency of the gun is therefore about 1.1%. Almost all of the current is dissipated on the defining aperture and d.c. operation would result in a delivery of about 235 watts of beam power to this electrode. It is therefore necessary in order to prevent damage to pulse the gun on and off.

Modulation of the gun

The method of modulation is indicated in figure 3. A thin non-intercepting grid at the correct space potential has no effect on the electron optics of the gun and is therefore used. Its position z_g in front of the cathode is calculated from the formula

$$\frac{\Phi_g}{\Phi_A} = \left(\frac{z_g}{d}\right)^{4/3} \qquad (19)$$

A reasonable value for the "on" potential is 1 of Φ_A ie Φ_g = 650 volts. This results in a value of $z_g/d = 0.032$ and a cathode grid spacing of 0.080 cm. Figure 6 indicates the spatial relationship between the control grid the cathode and the focus electrode. It is evident that the penetration of the anode field will be small so that the gun will cut off rapidly with a small negative bias. This should not exceed - 150 volts with respect to the potential of the cathode. The slit in the control grid is 0.30 mm wide and is designed to permit more than 99% of the beam current to pass through with the grid at the "on" potential.

Mechanical Design

Design of the electron gun

A schematic representation of the gun is given in figure 7. Considerable attention has been given to the problem of voltage breakdown to ensure that critical spacings between electrodes, along ceramics and from the cathode region to the wall of the vacuum versee are maintained. We envision the incorporation of two sets of deflection plates into the drift space between the anode and the first electrode of the unipotential lens to center the beam on the trimming aperture and to ensure normal incidence. In addition because of the tight mechanical tolerances the slits in the electrodes will be movable with respect to the focus electrode and grid electrode. Figure 8 shows the mechanism used to translate the electrodes.

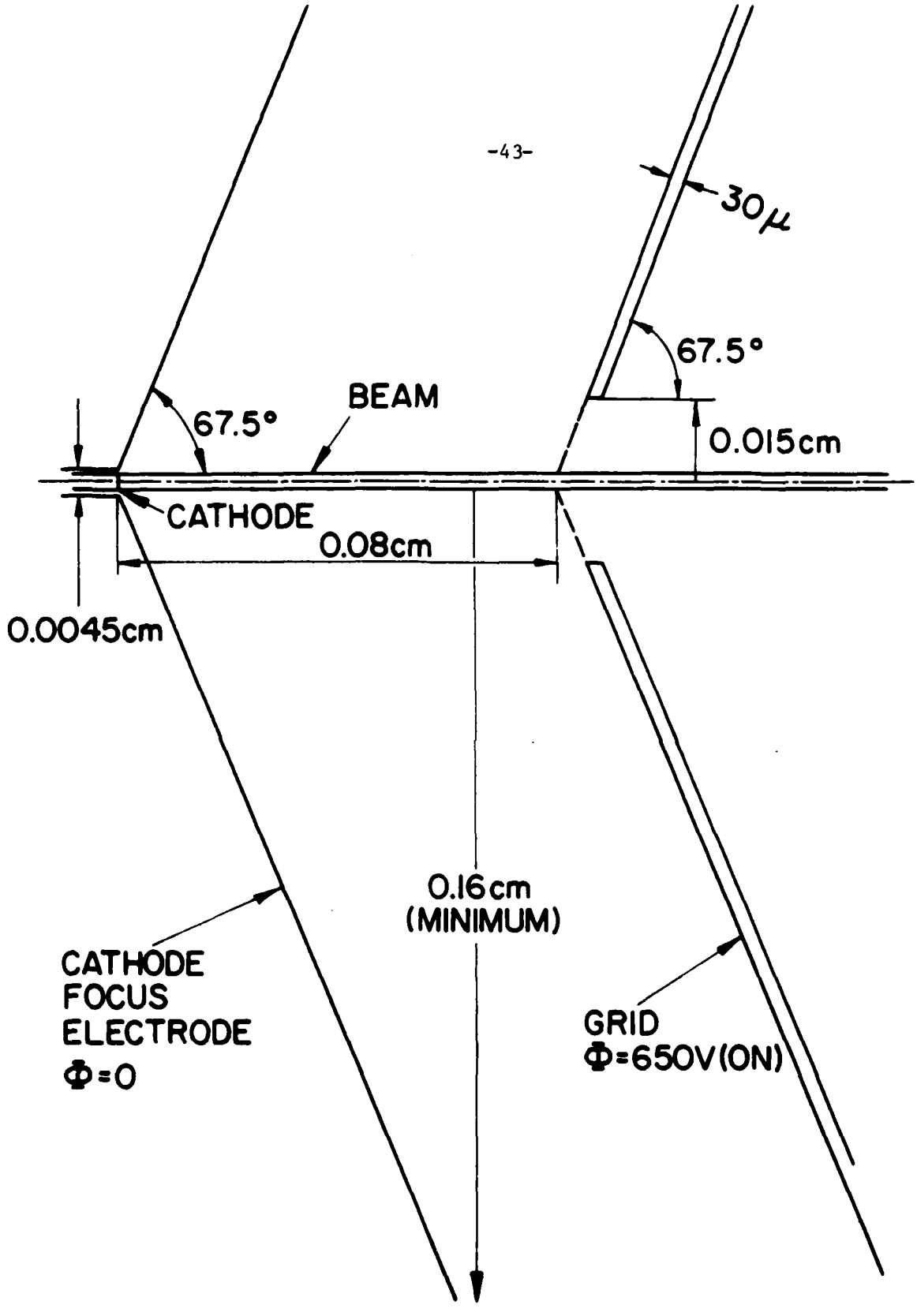

FIG. A-6

LOCATION OF CONTROL GRID WITH RESPECT TO CATHODE

Design of the LaB_6 cathode and heater

The major disadbantage of Lanthanum Hexaboride is the corrosive reaction at high temperature which occurs between it and most materials which would normally be considered to be useful cathode supports. Only carbon appears to be a non-reactive support. Thus the problem of mounting and supporting the cathode in the focus electrode presents a major challenge. Accordingly we are adopting several approaches to the cathode-heater design problem.

a) We are purchasing a standard LaB_6 cathode mounted on a carbon "spring" from Kimball Physics for use in our initial experiments and to determine the mechanical stability of this design. Figure 9 shows the Kimball design, according to their brochure. The design is attractive since it uses a very small amount of heater power which is in the order of 6 watts.

b) We are conducting experiments to design a LaB_6 cathode, mounted in a stable configuration on carbon machined from 5890 graphite (made by ...) . Initial experiments indicate that a heater power in excess of 40 watts may be required.

c) The third approach we are considering is that devised by Broers. In this a long LaB_6 rod is mounted a copper heat sink as shown in figure 10 and the upper end is radiation and electron bombardment heated. This

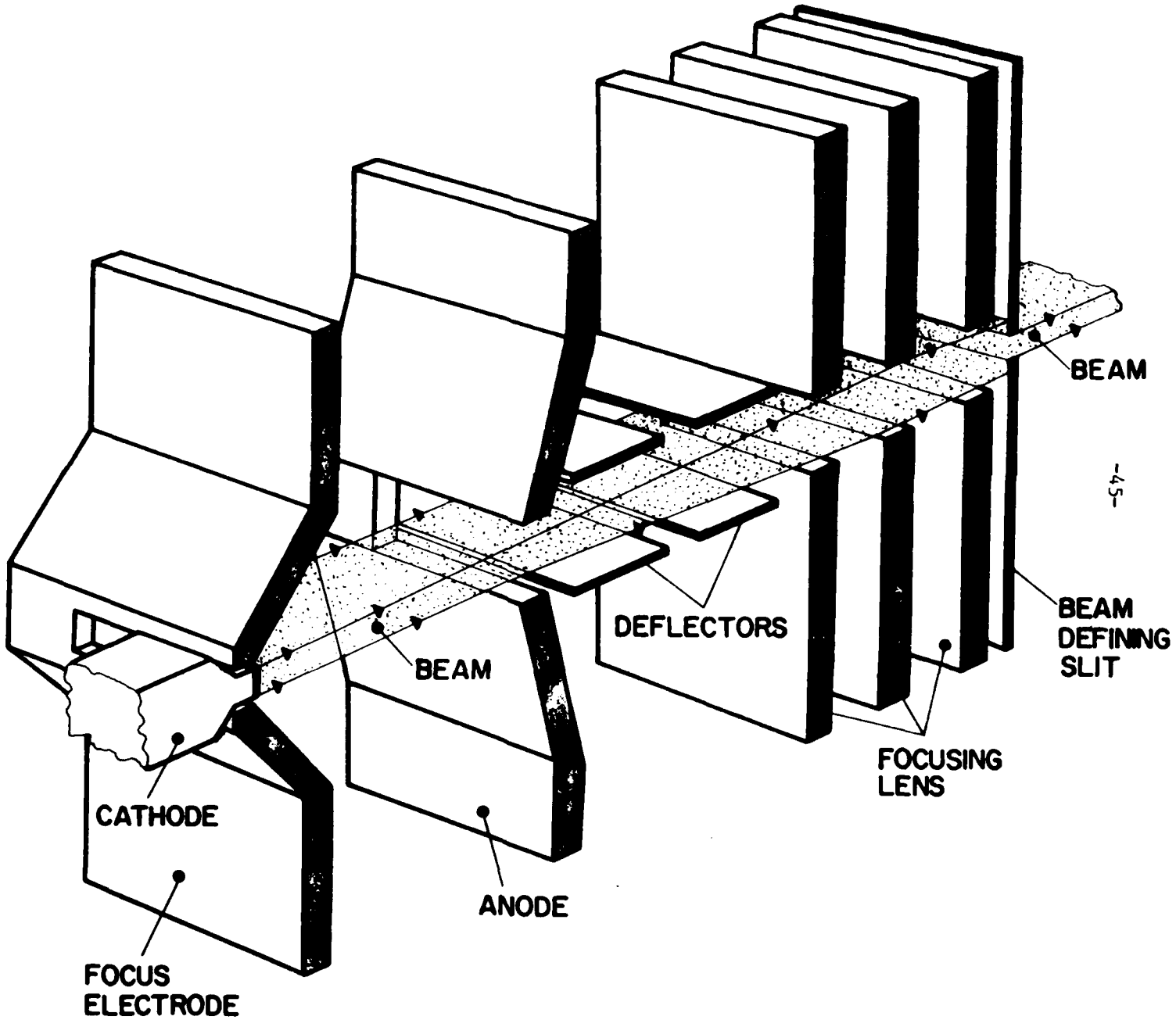

FIG.A7 ELECTRON GUN FOR PRODUCING THIN RIBBON-LIKE BEAM.

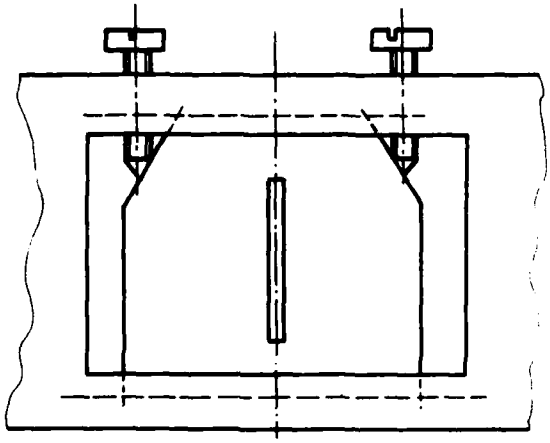

FIG. A8

SHEET APERTURE TRANSLATING MECHANISM

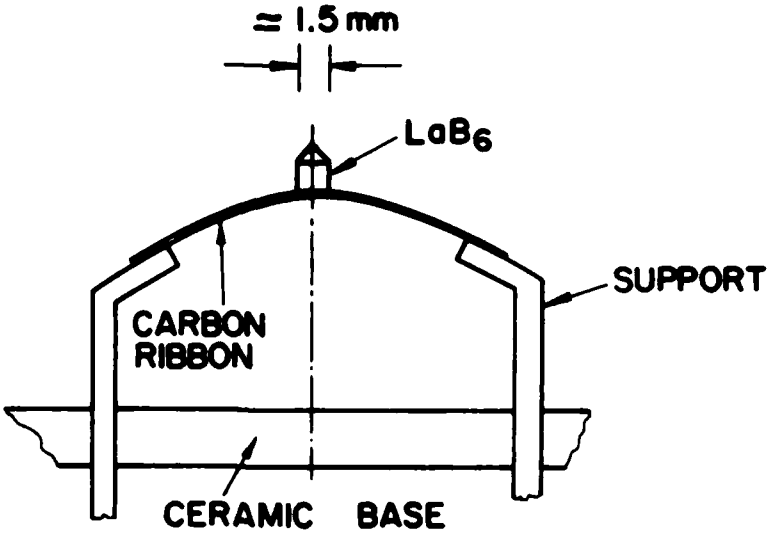

FIG. A9

LaB_6 CATHODE AND HEATER DESIGNED BY KIMBALL PHYSICS

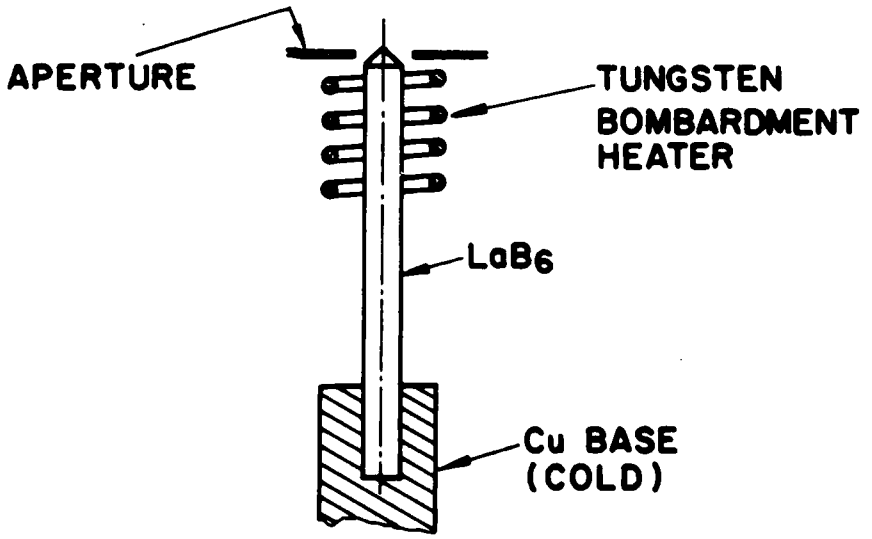

FIG. A10

BOMBARDMENT HEATER LaB_6 CATHODE

design is used successfully in scanning electron microscopes. It's main disadvantage appears to be the need for a bombardment power supply floated at cathode potential.

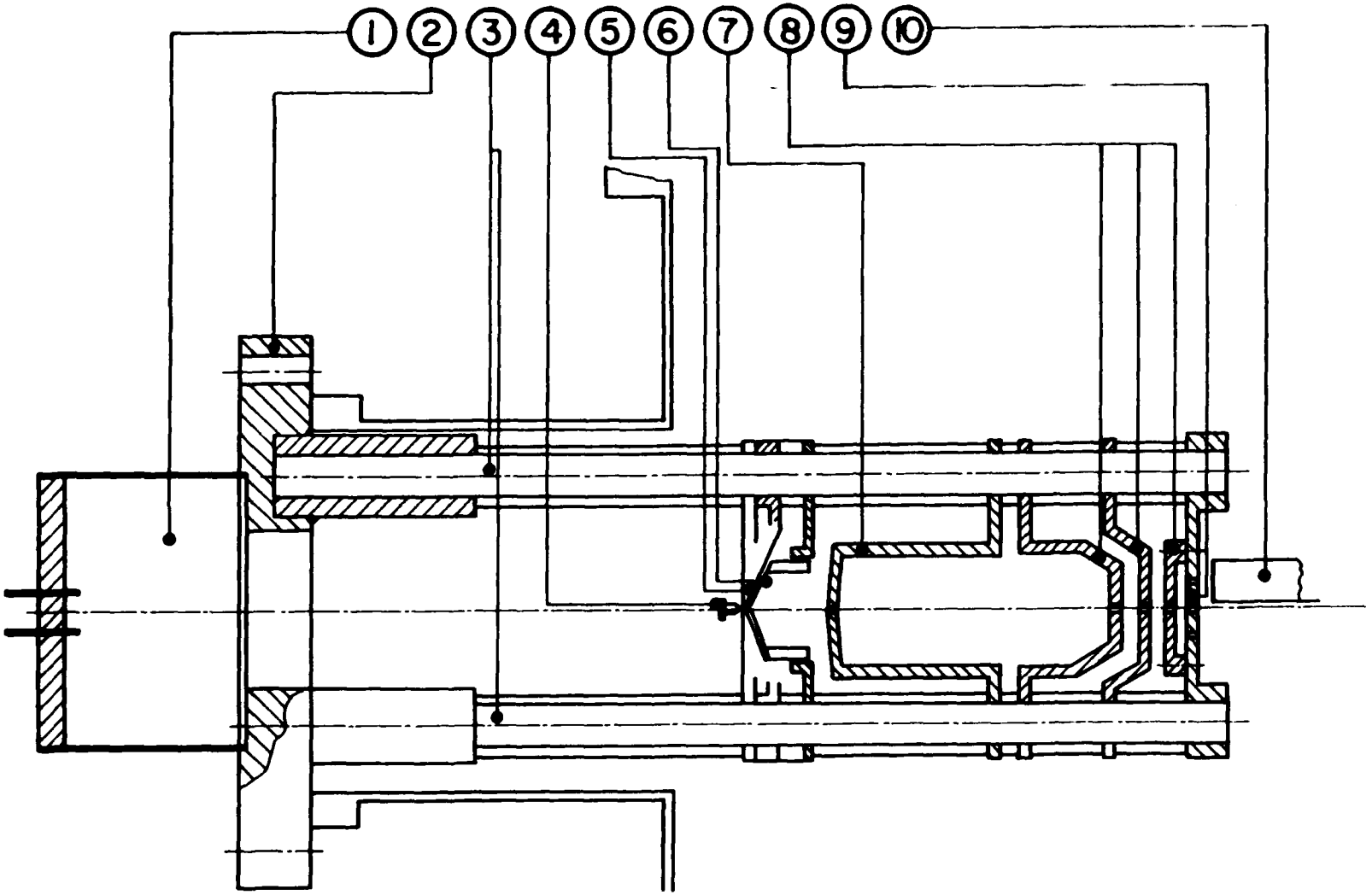

Fig. A-11: Mechanical design of E-gun no. 2:

(1) H.V. feedthrough (2) 6" conflat flunge (3) ceramic rods (4) cathode (cathode alignment assembly not shown) (5) beam forming electrode (6) grid (7) anode (8) electrostatic lens (9) slit assembly (10) sample

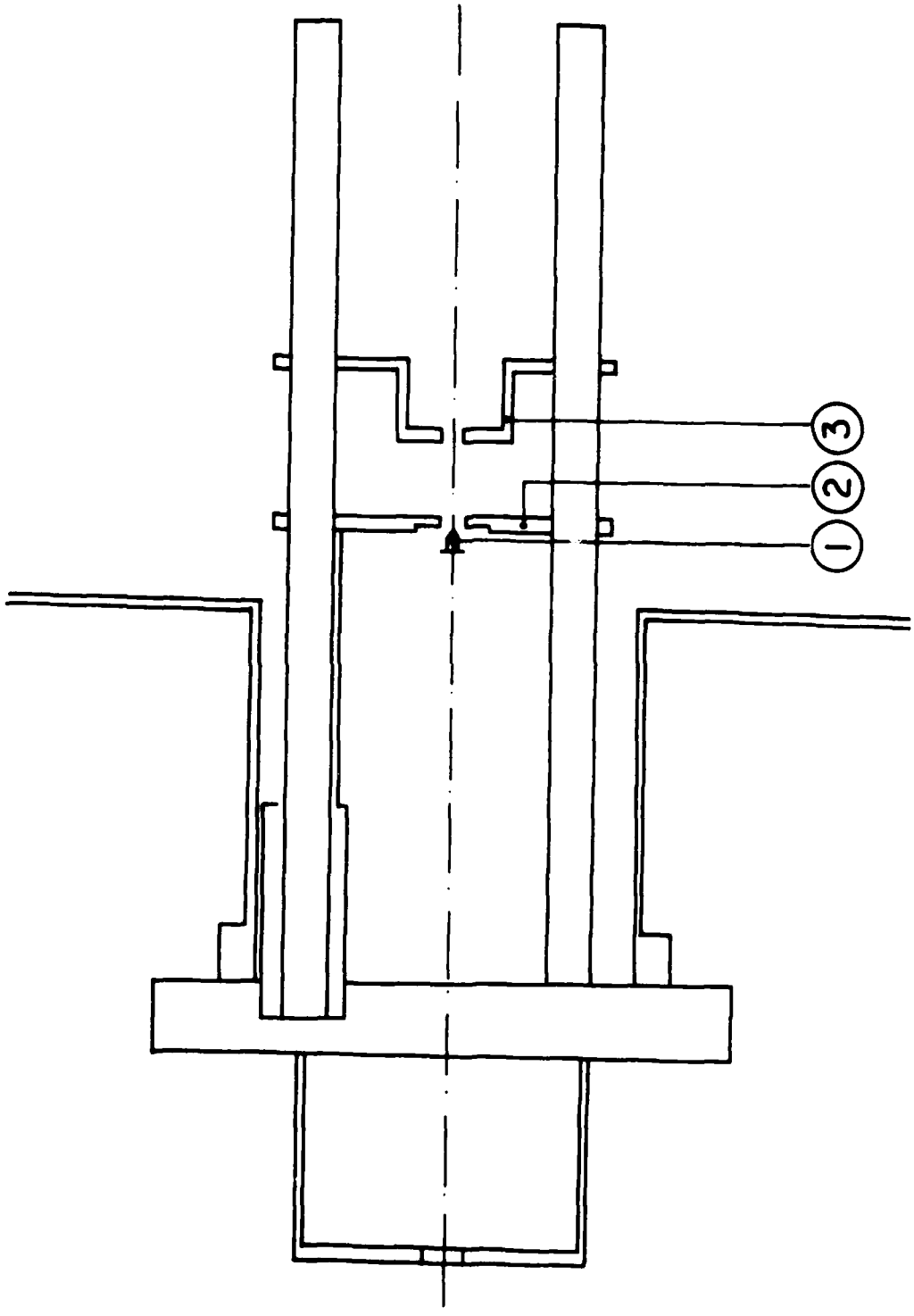

Fig. A-12: Mechanical design of e-gun no. 1A (1) cathode (2) grid (3) anode

Appendix B: Simulation of Electron Guns - Mordechai Landau

Introduction

We are using the SLAC electron optics program for simulating our electron guns. This program was written in Stanford by W.B. Hermansfeldt. We are doing simulation for the following reasons:

A. Planning the electron gun is made by using well known formulae of the electron optics. Unfortunately this theory gives exact results for only few configurations. So these configurations are used as the basic forms for the planner, and every change must be tested numerically. For example, in our gun (no. 2) there is a unipotential lense and we could not find formula for its focal length. The formulae in the literature are evident for cylindrical symmetry and not for planar symmetry.

B. Simulation enables one to check the approximations made in the theoretical analysis.

C. Using the program, one can check the results of changing parameters like applied voltages and distances between parts of the electron gun.

How the program works

The program can work only on guns which have cylindrical or planar symmetry, so the problem can be described two-dimensionally. Nevertheless, some information on the third dimension can take part in the calculations

and appear in the results.

The trajectories of the electrons in the gun are calculated iterativly with two steps:

A. First, the electric potential everywhere inside the gun must be found from the given data about the potential on the boundaries and the calculated charge inside the gun. The physical solution is given by a differential equation (Poisson's equation). The program solves this equation by dividing the area by a mesh and transferring the differential equation into a set of linear equations. This is the finite-difference method. The set of linear equations is solved using the Gauss-Seidel method.

B. Now that the potential is known the program uses Lorentz equation to find the trajectories.

Using the program for our gun

We had to solve two problems in order to use the program:

A. The program was written to run with I.B.M. 370 Computer while we have a C.D.C. 6800 Computer. Many changes were required in order to enable using the program. A major modification was required in order to run the plotter subrutines.

Another change was the replacing of a double-precision order by a single precision. This change did not caused a loss of accuracy because an I.B.M. word is of 32 bits while a C.D.C. word is of 60 bits. So one C.D.C. word has bits almost as many as two I.B.M. words.

B. The maximum area the program can deal with in the same time is 9000 mesh points. (Changing the program in order to enlarge the area is not possible in our computer). But our electron gun is complicated and has many details. This forces us to divide the gun to five parts. The program finds the trajectories in the first part and then delivers the results as initial conditions to the next part.

The results

The output of the program includes a written output and plots. The written output includes a map of the potential distribution, the expected current, and the energy and direction of the current flow trajectories in the end of the part analysed.

The plots are of the trajectories inside the part (see figures 1 and 2) and the profile and direction in the end of the part. Figures 1 and 2 demonstrate an example of the use of the program to analyse the gun. The gun analysed is e-gun no. 2 shown in fig. A-3, starting from the cathod and grid electrodes, through the anode to the unipotential lense. In figure 1 we see the electron trajectories emitting from the cathod. As is expected from the theory the beam focusing pierce electrode which is shaped at 67.5° half opening angle forces the electrons to go straight. In figure 2 we see the effect of the unipotential lense on rays entering horizontally to this part and can find the focal length.

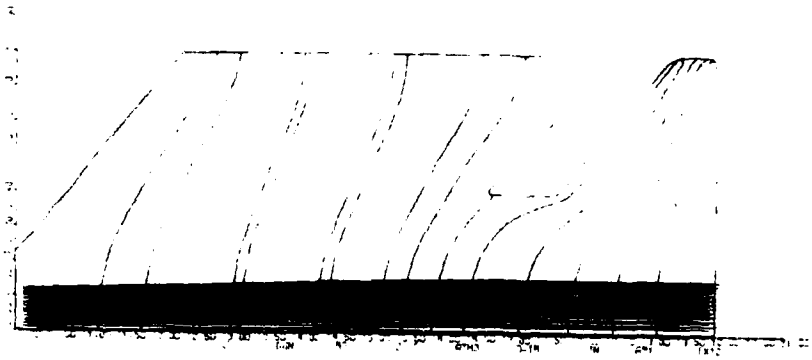

Fig. B-1: Computer drawing of computed electron trajectories in gun no. 1 in the region between cathode to anode.

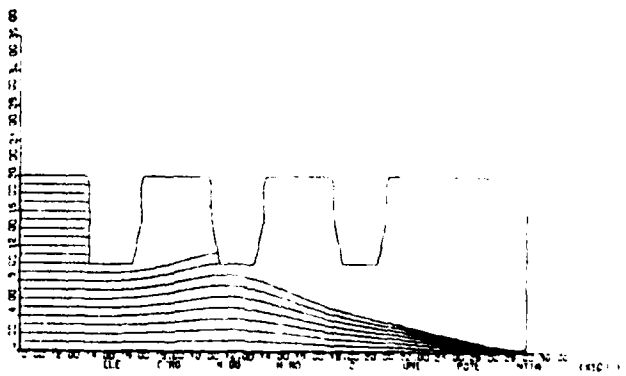

Fig. B-2: Computer drawing of computed electron trajectories showing the focussing effect of the electrostatic lens of gun no. 2.

APPENDIX C: Waveguiding experiments at 10.6 μm wavelength - Paul Dvorkis

a) Introduction

In the previous progress report (dated February 28th 1979), the theory of Hollow Dialectric waveguides was reviewed [4] and we reported some experimental measurements of attenuation versus mode "zig-zag angle" through hollow dialectric waveguides.

The reason for wanting to achieve high "zig-zag angle" modes with moderate losses in hollow dialectric waveguides is the following: The interaction of an electron beam with an electromagnetic wave can take place in a waveguide with a slow wave structure where the phase velocity of the electromagnetic mode is approximately the same as the group velocity of the electron beam. However, the interaction takes place through the longitudinal electric component E_z of the electromagnetic mode. Since low order hollow dialectric waveguide modes have a very small E_z component, we should prefer to use high order modes (which means high "zig-zag angle").

In our last report we suggested a waveguide structure which allows moderate losses of high order modes. This structure is illustrated in Fig. C-1. The wide sides of width b are made of a conducting material and the narrow sides (thickness a) can be either conducting or a dielectric material like glass.

Three waveguides of the kind illustrated in Fig. C-1 were constructed:

waveguide no. 1: $a \times b \times \ell = 1 \times 5.3 \times 76$ mm^3 sides a - glass
sides b - stainless-steel.

waveguide no. 2: $a \times b \times \ell = 0.1 \times 0.5 \times 60$ mm^3 sides a - glass
sides b - stainless-steel.

waveguide no. 3: $a \times b \times \ell = 0.4 \times 3 \times 70$ mm^3 sides a - aluminum,
sides b - aluminum.

The stainless-steel and aluminum walls were comercially available polished materials. The glass walls (1 mm and 0.1 mm thick) were microscope slides, hand polished in our laboratory.

The power attenuation constant of a plane wave bouncing at a "zig-zag angle" ϕ at the a walls with P polarization (polarization parallel to the plane of incidence which is parallel to the b walls) as shown in Fig. C-1 is:

$$\alpha = \frac{\lambda^2}{a^3} \text{Re}\left[\frac{1}{\sqrt{\nu_a^2 - 1}}\right] + \frac{\lambda^2}{b^3} \text{Re}\left[\frac{\nu_b^2}{\sqrt{\nu_b^2 - 1}}\right] \left(\frac{\phi}{\phi_o}\right)^2 \qquad (1)$$

where $\nu_a = n_a - ik_a$ is the complex refractive index of the wall made of material a; $\nu_b = n_b - ik_b$; and $\phi_o = \lambda/2b$.

If the radiation is S polarized (perpendicular to the plane of incidence - or parallel to the a walls) then:

$$\alpha = \frac{\lambda^2}{a^3} \text{Re}\left[\frac{\nu_a^2}{\sqrt{\nu_a^2 - 1}}\right] + \frac{\lambda^2}{b^3} \text{Re}\left[\frac{1}{\sqrt{\nu_b^2 - 1}}\right] \left(\frac{\phi}{\phi_o}\right)^2 \qquad (2)$$

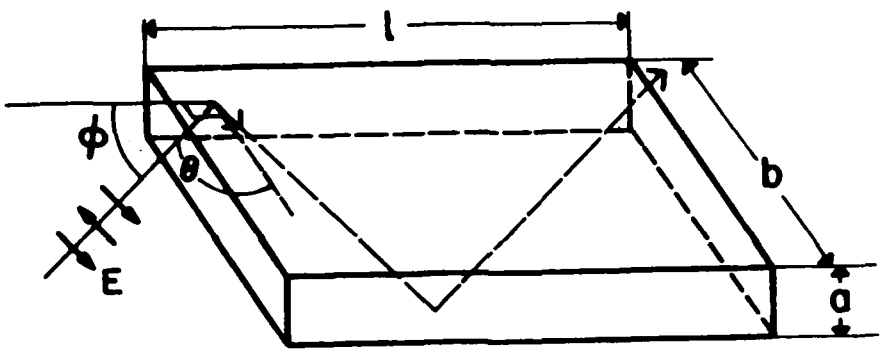

Fig. C-1: Configuration for hollow dielectric waveguiding experiments with a << b, "zig-zag angle" ϕ of an incident plane wave bouncing at the a walls and P polarization (polarization parallel to the plane of incidence).

b) Evaluation of refractive index at 10.6 μm

The refractive index of glass [5] is $\nu = 2.1 - j\ 1.2$ which gives us:

$$\text{Re}\left(\frac{1}{\sqrt{\nu^2-1}}\right) = 0.358 \ ; \ \text{Re}\left(\frac{\nu^2}{\sqrt{\nu^2-1}}\right) = 2.27$$

From another source we get for Pyrex glass $\nu = 1.91 - j\ 0.077$ which gives us:

$$\text{Re}\left(\frac{1}{\sqrt{\nu^2-1}}\right) = 0.616 \ ; \ \text{Re}\left(\frac{\nu^2}{\sqrt{\nu^2-1}}\right) = 2.24$$

For aluminum we have [6] $\nu = 20.5 - j\ 586$, while another source [7] claims $\nu = 25 - j\ 67$. For stainless-steel we did not find any reference. For this reason, and also because value of the complex refractive index of the other materials could depend on the purity and manufacturing processes of the materials used, we made our own measurements of complex index of refraction by measuring single reflection losses from a plane surface as a function of incidence angle and polarization.

To calculate the complex refractive index ν we use the expression for Single-Reflection-Loss at Grazing Incidence angle ϕ:

$$L_S = L_\perp = 4\ \phi\ \text{Re}\left(\frac{1}{\sqrt{\nu^2-1}}\right) \tag{3}$$

$$L_p = L_\parallel = 4\ \phi\ \text{Re}\left(\frac{\nu^2}{\sqrt{\nu^2-1}}\right) \tag{4}$$

where $L_\perp$ and $L_\parallel$ are the loss factors at S and P polarization respectively (perpendicular or parallel to the plane of incidence respectively).

Thus from measuring Single Reflection Loss at Grazing Incidence $\phi = 90° - \theta \to 0$ (θ is the angle of incidence measured from the normal to the surface) one can get the parameters we need.

The results of such measurements are shown in Fig. C-2 for glass, Fig. C-3 for stainless-steel and Fig. C-4 for aluminum.

From Fig. C-2 we get for glass:

$$\mathrm{Re}\left(\frac{\nu^2}{\sqrt{\nu^2-1}}\right) = 3.4 \pm 0.5 \quad ; \quad \mathrm{Re}\left(\frac{1}{\sqrt{\nu^2-1}}\right) = 0.4 \pm 0.1$$

For metals which have $n_1 k \gg 1$, $|n-k| \gg 1$ (where $\nu \equiv n - ik$) we have $\mathrm{Re}\,\frac{1}{\sqrt{\nu^2-1}} \simeq \frac{n}{n^2+k^2} \ll 1$ and thus the Single Reflection Loss at Grazing Incidence for S polarization is too small to be measured. In this case we use for calculating the complex index ν, the normal incidence Fresnel reflection formula [8]

$$L(\theta = 0°) = \frac{4n}{(n+1)^2+k^2} \tag{5}$$

where $L(\theta = 0°)$ is the Power reflectivity at normal incidence.

From Fig. C-3 we calculate that

$$\nu(\text{stainless-steel}) = (29 \pm 1) - j(36 \pm 2)$$

From Fig. C-4 we calculate

$$\nu(\text{aluminum}) = (20 \pm 1) - j(48 \pm 2)$$

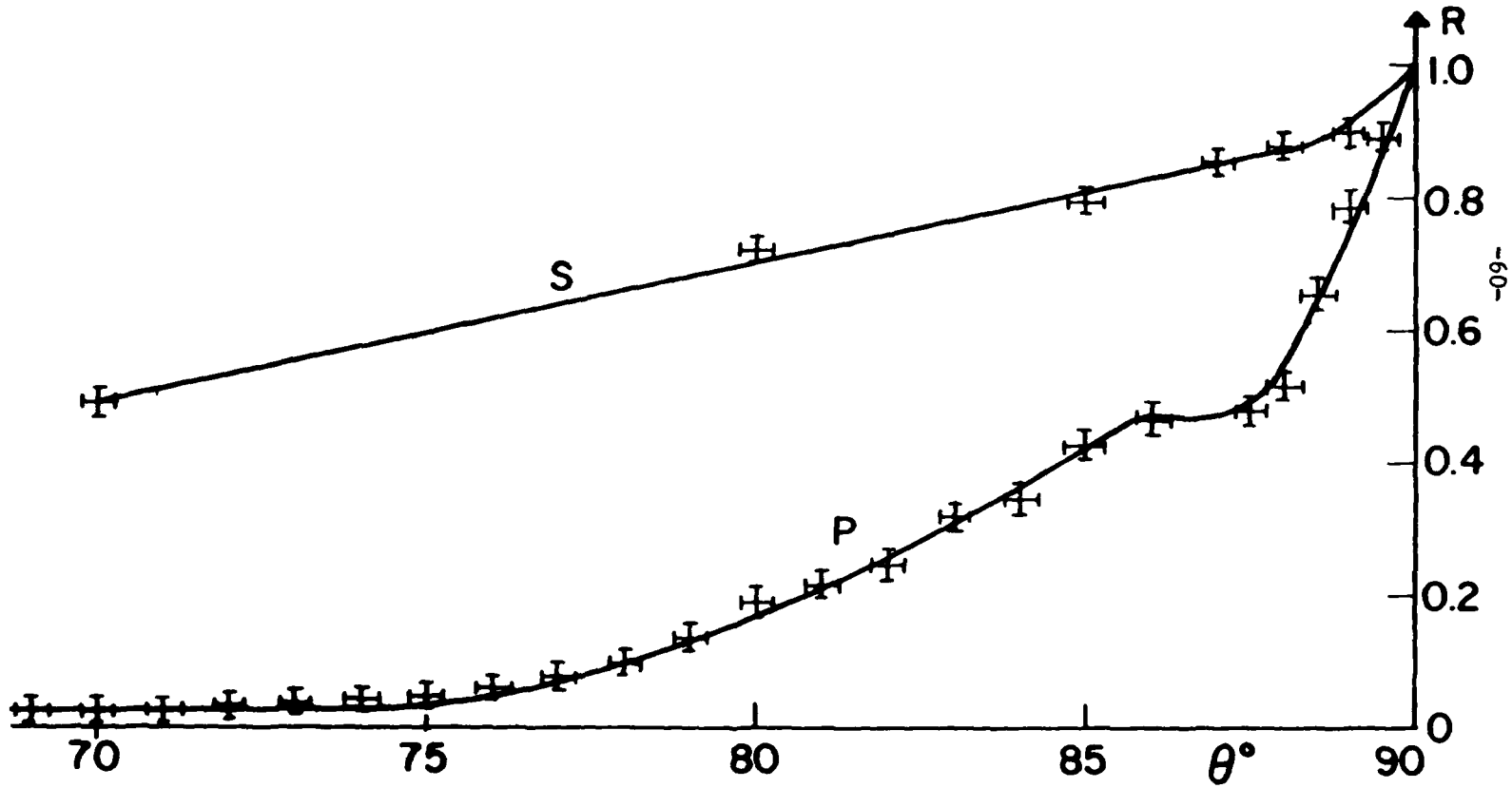

Fig. C-2: Reflectivity R of a glass surface versus angle of incidence θ for S and P polarizations.

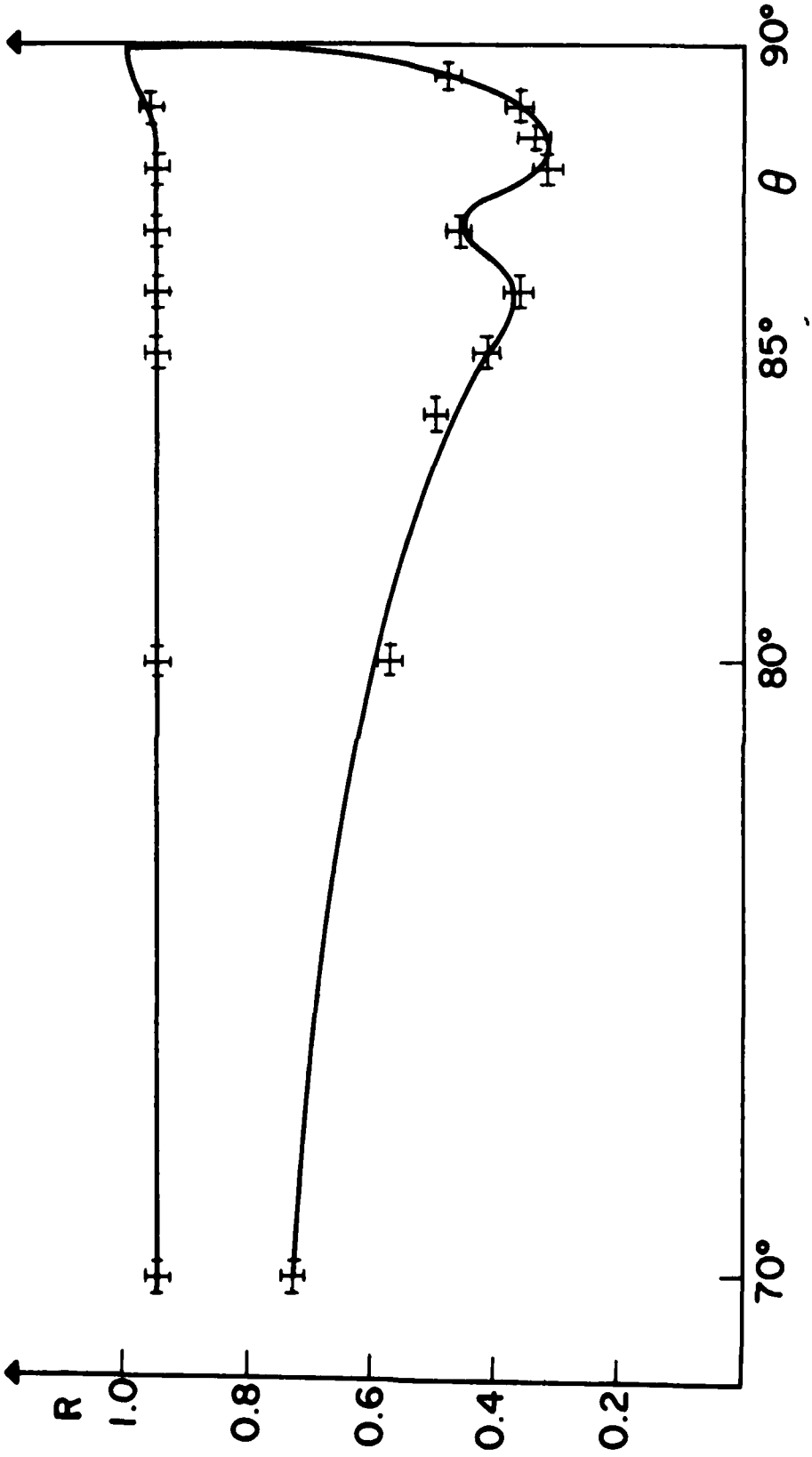

Fig. C-3: Reflectivity R of a stainless-steel surface versus angle of incidence θ for S and P polarizations.

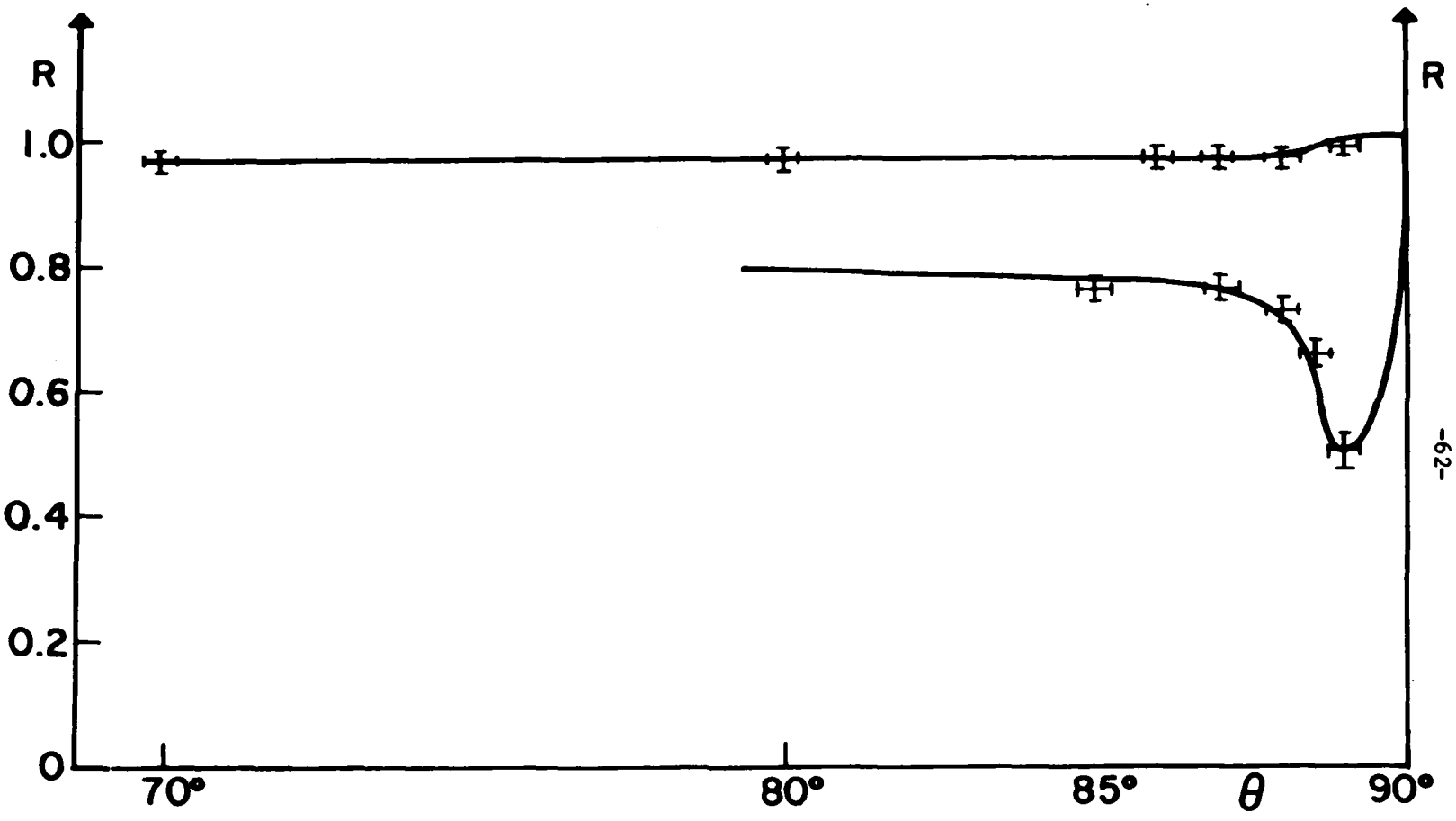

Fig. C-4: Reflectivity R of an aluminum surface versus angle of incidence θ for S and P polarizations.

c) "Zig-Zag Angle" dependence of attenuation in waveguide

In Figures C-5, C-6 and C-7 we show the measured power transmission through waveguides no. 1 and 2 (respectively) versus "zig-zag angle" θ. The transmission shown in those Figures is normalized to the maximum transmission ($\phi = \phi_o$).

The theoretical curves in these Figures, are obtained using equations (1) or (2). The complex refractive index used in the equations is calculated in part b of this report from measurements shown in Fig. C-2, C-3, C-4.

As one can see from Fig. C-6 in waveguide no. 1 we had a fairly good transmittance up to $\phi \simeq 18°$ which is quite encouraging.

In waveguide no. 2 (100 μm thick!) we had fairly good transmittance for S pol. (up to $\phi \simeq 8°$). However, in that waveguide, attenuation for P polarization ($\vec{E}$ perpendicular to the stainless-steel wall) was so high even for $\phi = \phi_o$ that we did not included it in Fig. C-7.

d) A comment on the limits of validity of the theory of Ref. [4]

The discrepancy between the experimental points and the theoretical curve in Fig. C-7 led us to believe that the approximation (on which this theory is based), is not valid any more. The validity criterion of eq. (1) and (2) can be written in our waveguide configuration:

$$\frac{4b}{\lambda} >> |\nu|\, m \qquad (6)$$

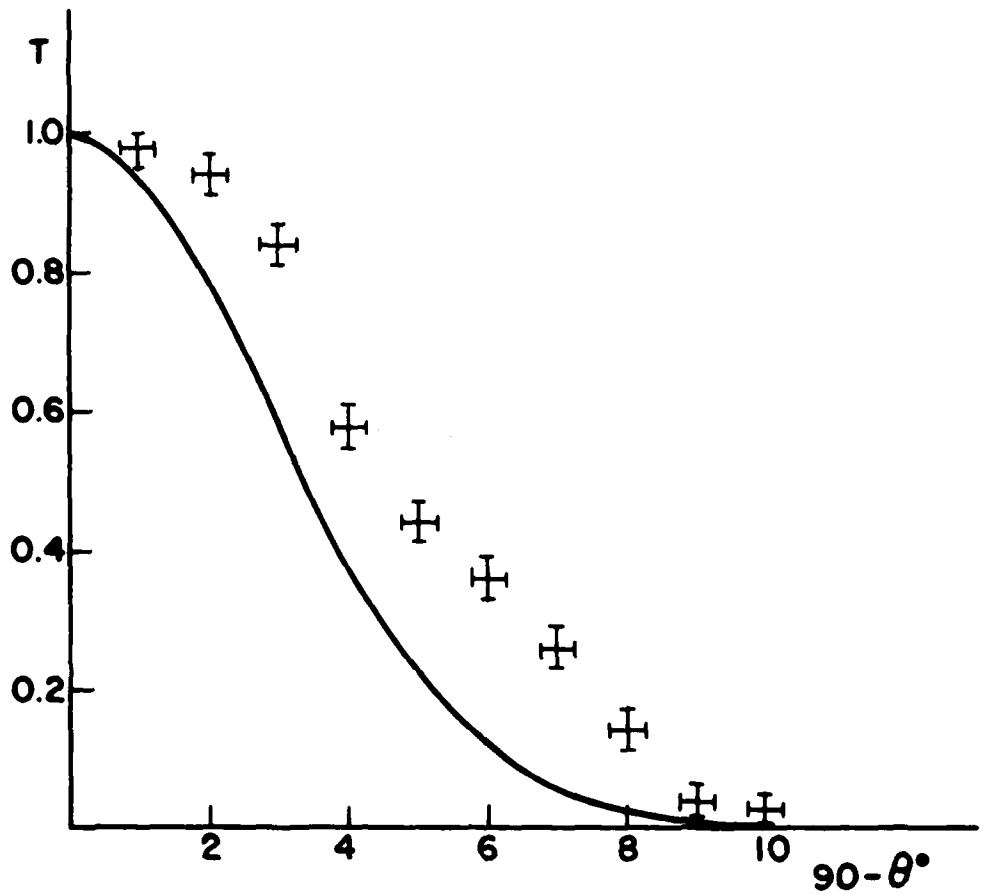

Fig. C-5: Transmission T of waveguide no. 1 versus angle $\phi = 90° - \theta$ for P polarization (exactly the same configuration as illustrated in Fig. 1). The solid line is calculated according to eq. (1). Both theoretical and experimental results are normalized to the maximum transmission (where $-\phi_o \leq \phi \leq \phi_o$).

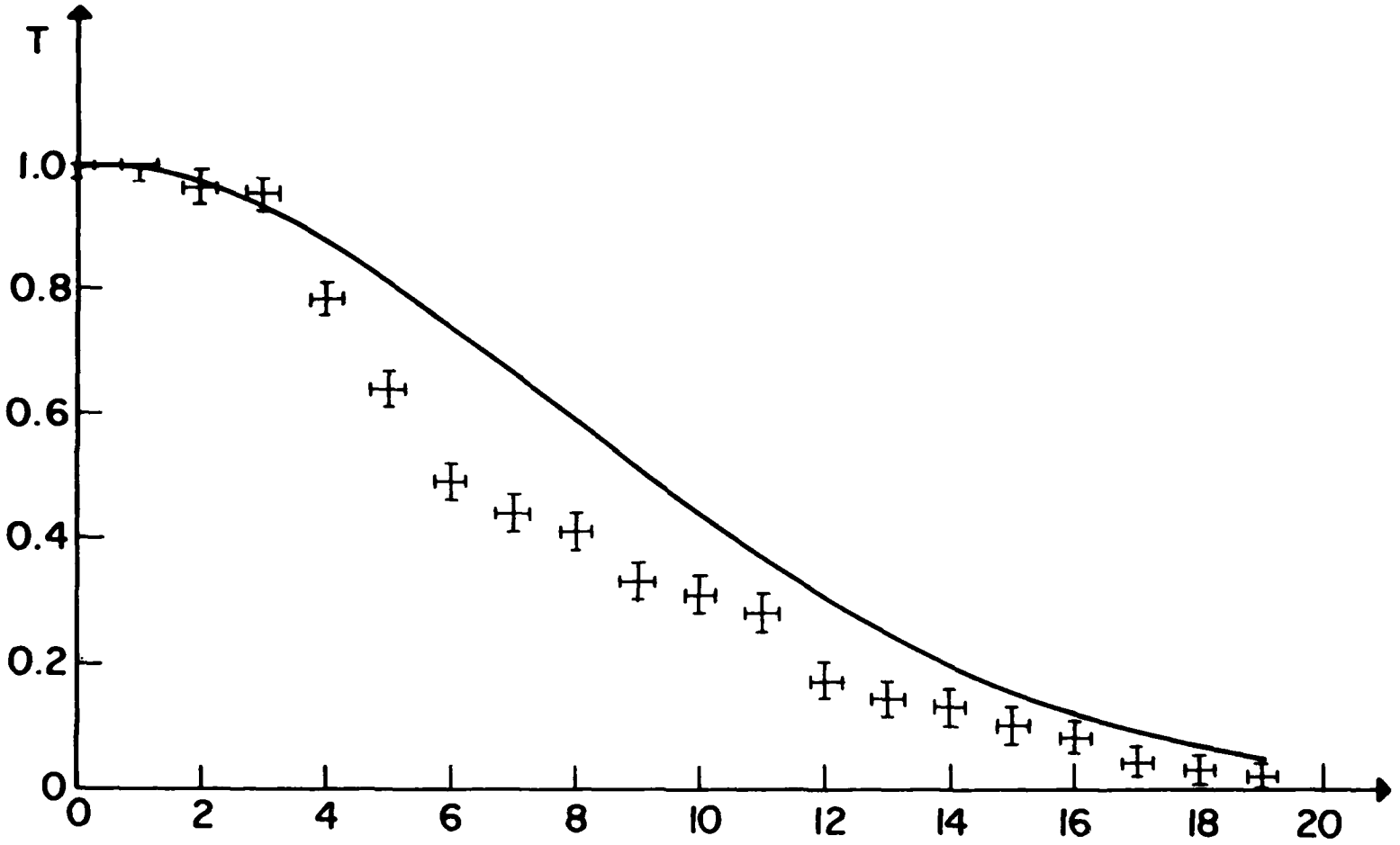

Fig. C-6: Transmission T of waveguide no. 1 versus angle $\phi = 90° - \theta$ for S polarization ($\vec{E}$ is perpendicular to the b walls made of stainless-steel). The solid line is calculated according to eq. (2). Both theoretical and experimental results are normalized to the maximum transmission ($-\phi_o \leq \phi \leq \phi_o$).

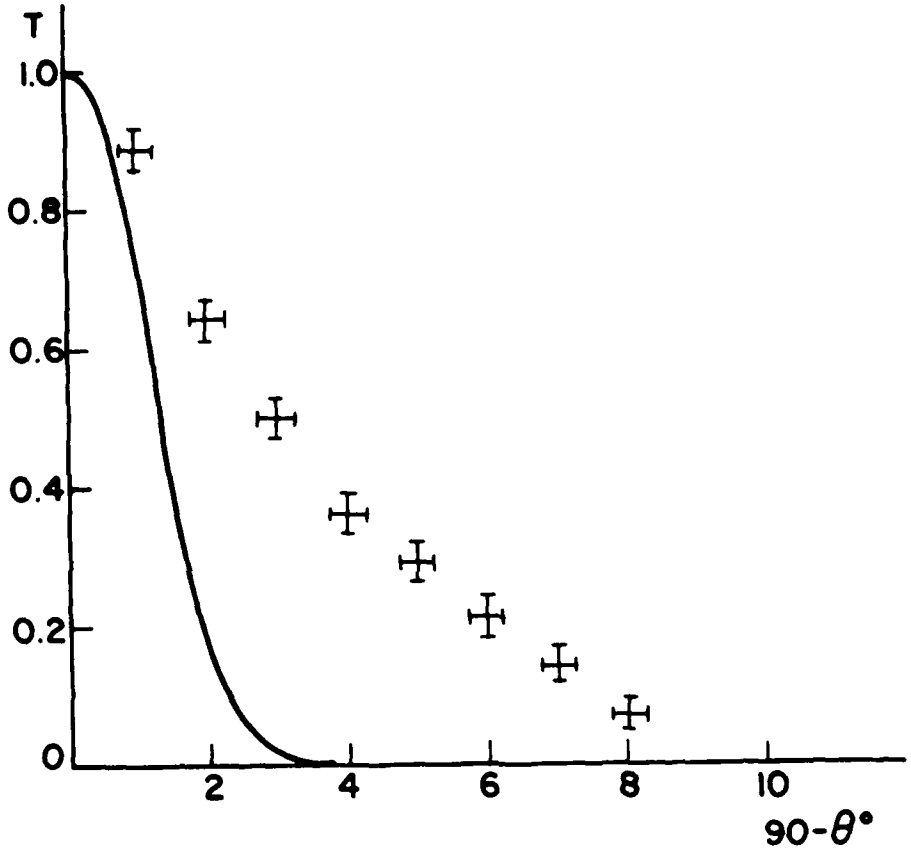

Fig. C-7: Transmission T of waveguide no. 2 versus angle $\phi = 90° - \theta$ for P polarization (the same as in Fig. 1). The solid line is calculated according to eq. (1). Both theoretical and experimental results are normalized to the maximum transmission $(-\frac{\phi_o}{2} \leq \phi \leq +\frac{\phi_o}{2})$.

where m is the waveguide mode order number corresponding to the axis whose lateral waveguide dimention is b, and can be expressed in terms of the "zig-zag angle" ϕ as $\phi/\phi_o \simeq m$ and thus we require that:

$$\frac{4b}{\lambda} >> |\nu| \, \phi/\phi_o \tag{7}$$

In waveguide no. 2 we have $b/\lambda \simeq 50$ $|\nu_{glass}| \simeq 3.5$, $\phi_o = \lambda/2b = 0.6°$ and thus we need that $\phi << 34°$ however the experimental data deviates from the theoretical curve (Eq. 1) already at $\phi > 2°$ (Fig. C-7).

In order to examine a more distinct case where inequality (7) is not satisfied, we measured attenuation of waveguide no. 1 (in the configuration shown in Fig. C-8) versus "zig-zag angle" for P Polarization ($\vec{E}$ is parallel to the glass walls).

The experimental data and theoretical curve are presented in Fig. C-9. In the configuration of this experiment, we need that $\frac{4a}{\lambda} >> |\nu| \, (\phi/\phi_o)$ $|\nu_{S.S.}| \simeq 46$, $\phi_o = \lambda/2a = 0.3°$, $a/\lambda \simeq 100$ and thus $\phi << 2.6°$. As one can see from Fig. C-9 for $\phi > 0.5°$ the experimental transmission is much higher than the theoretical prediction. A fact that strongly suggest that the theory is no longer applicable in the high order modes or low a/λ regimes.

We constructed a third waveguide (no. 3) made of aluminum with $a = 400$ μm and measured attenuation versus angle in the configuration of Fig. C-8.

In this waveguide even at the minimum angle $\phi = \phi_o$ the approximation does not hold, $a/\lambda = 40$; $|\nu_{A1.}| \approx 52$; $\phi_o = 0.75°$ and we need $\phi << 2.3°$.

The results of the experiment with waveguide no. 3 are presented in Fig. C-10 and one can clearly see that the "grazing angle" approximative equations do not hold here.

Another experiment which we made was to measure minimum waveguide losses for P polarization as in Fig. C-8, for the 3 waveguides we measured. Those points are presented in Fig. C-11 and one can see that for $\phi = \phi_o = \lambda/2a$ the theory does not hold when $a < 1$ mm.

The same measurements for aluminum waveguides but with S polarization ($\vec{E}$ parallel to the longer metalic wall) were performed in Ref. [9] and the same discrepancy below $a < 1$ mm was encountered (Ref. [9] - Fig. 1).

However, their interpretation was that their aluminum-material was not ideal, but a commercial one, which supposedly has different properties. We believe that the disagreement between experiment and theory results from inapplicability of the small grazing angle approximation (Eq. 1). We mean to fit the experimental data to expressions we developed which apply also to large "zig-zag angle" modes.

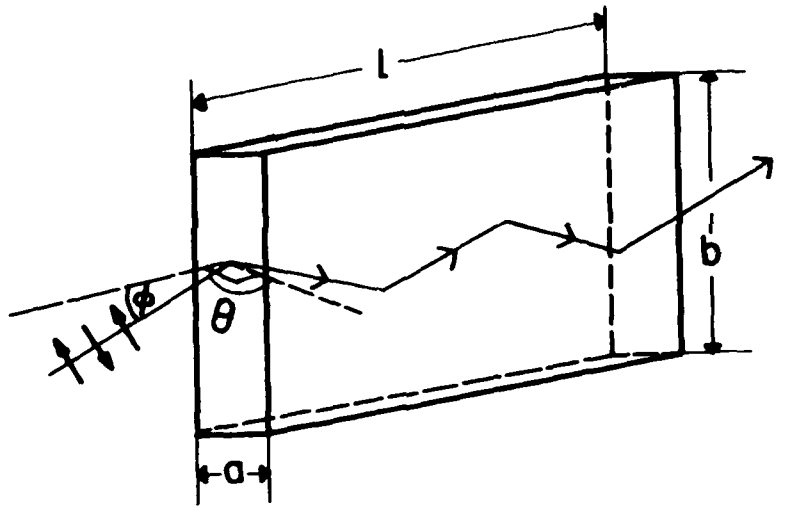

FIG. C-8

Fig. C-8: Configuration for hollow dialectric waveguiding experiments with a << b, "zig-zag angle" ϕ of an incident plane wave bouncing at the b walls with P polarization (parallel to the plane of incidence).

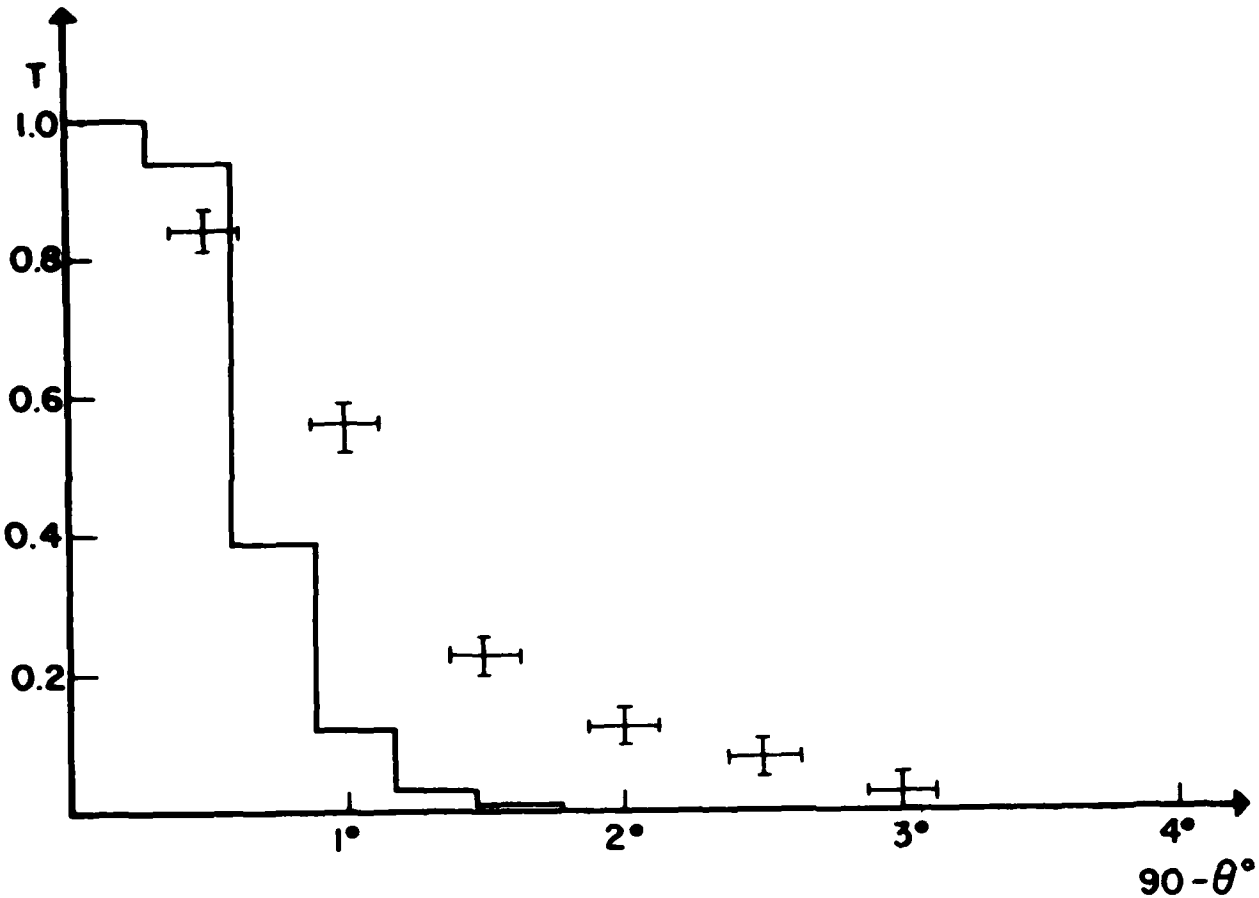

Fig. C-9: Transmission T versus angle $\phi = 90° - \theta$ for waveguide no. 1 in the configuration of Fig. C-8 (P polarization). The solid line is the attenuation (eq. (1)) quantized to the waveguide mode (ϕ is an integral multiple of ϕ_o).

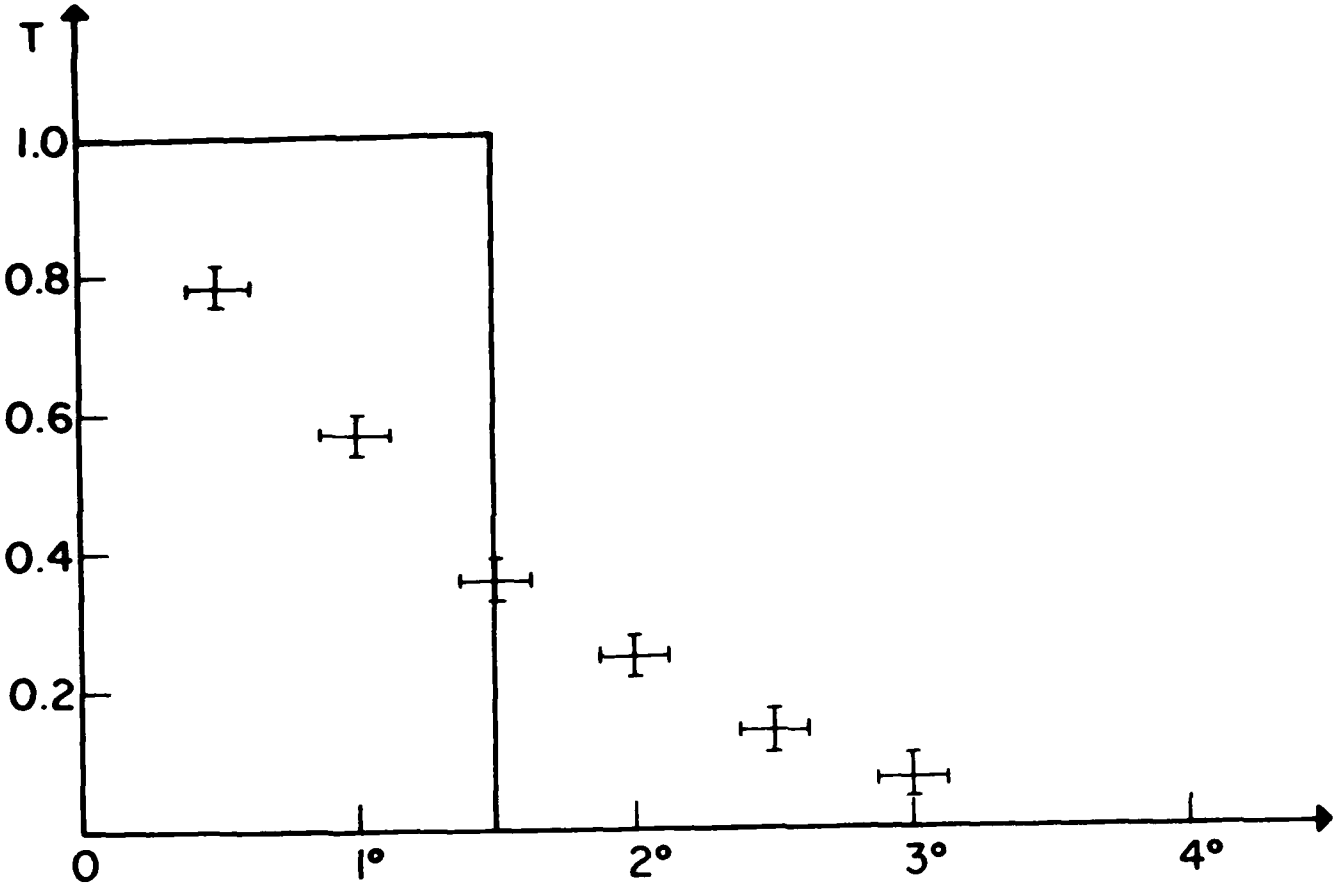

Fig. C-10: Transmission T versus angle $\phi = 90° - \theta$ for waveguide no. 3 in the configuration of Fig. C-8 (P polarization). The solid line is the attenuation (eq. (1)) quantized to the waveguide mode (ϕ is an integral multiple of ϕ_o).

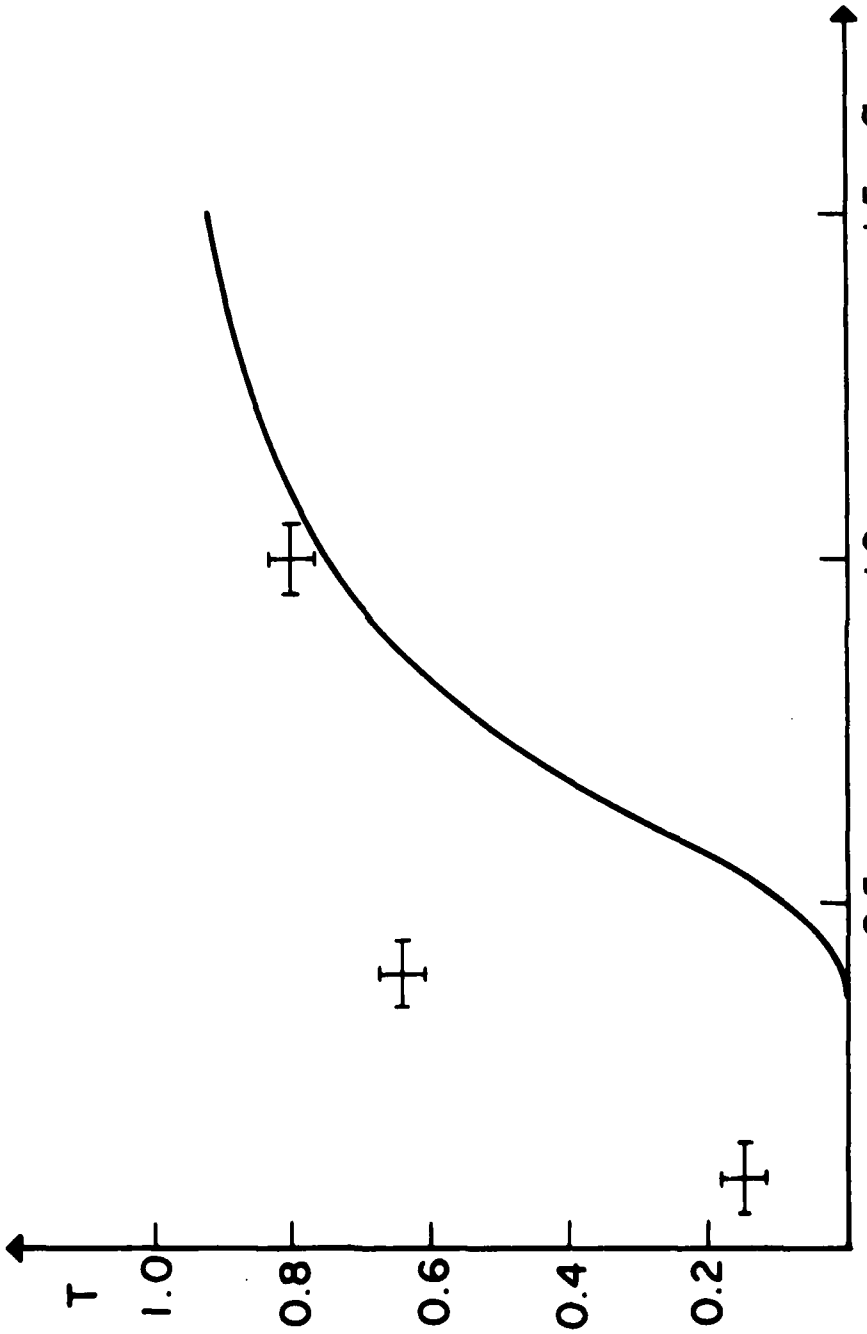

Fig. C-11:Maximum transmission T (ϕ = 0) versus waveguide dimension a for the 3 waveguides measured. The configuration is as in Fig. C-8 (P polarization). The solid line is calculated from eq. (1).

References

1. A. Gover "A Free Electron Laser Based on Periodic Longitudinal Electrostatic Bremsstrahlung". To be published in Physics of Quantum Electronics Vol. 7, S. Jacobs, Ed. Addison Wessley (1980).
2. A. Gover "An Analysis of Stimulated Longitudinal Electrostatic Bremsstrahlung in a Free Electron Laser Structure". Submitted for publication.
3. A. Gover and P. Sprangle "'Exact' Gain Expression for the Free Electron Laser and Effects of Transverse Velocity Spread and Incoherence of the Pump". Submitted for publication.
4. E.A.J. Marcatilz and R.A. Schmeltzer, Bell Syst. Tech. J., 43, p. 1783-1809 (July 1964).
5. W. Cleek, Appl. Opt. 5, 771 (1966).
6. J.R. Beattie, Philos. Mas. 46I, 235 (1955).
7. E. Garmire, T. McMahon and M. Bass, Appl. Opt. 15, 145 (Jan. 1976).
8. Born & Wolf, Principles of Optics, Pergamon Press (1975).
9. E. Garmire, T. McMahon and M. Bass, Appl. Phys. Lett. 29, 254 (August 1976).
10. H. Kogelnik and C.V. Shank, J. Appl. Phys. 43, 2327 (1972).
11. A. Gover and A. Yariv, Appl. Phys. 16, 121 (1978).
12. A. Gover and A. Yariv, Physics of Quantum Electronics, Vol. 5, p. 197 (S.F. Jacobs, M.S. Sargent III and M.O. Scully, eds., Addison Wesley Publishing Co. Inc., 1978).
13. A. Gover and Z. Livni, Opt. Commun. 26, 375 (1978).

14. Z. Livni and A. Gover, Linear Analysis and Implementation Considerations of Free Electron Lasers Based on Cerenkov and Smith-Purcell Effect. AFOSR 77-3445 Quantum Electronics Lab Scientific Report 1979. Tel Aviv University, January 1979.

15. A. Gover and P. Sprangle,"The Operating Parameters of Magnetic Bremsstrahlung, Electrostatic Bremsstrahlung and Cerenkov-Smith-Purcell Free Electron Lasers". In preparation.

16. Y. Carmel, S. Eylon and E. Shohet, J. Phys. E : Sci Instrum., Vol. 11, p. 748 (1978).

17. Y. Carmel and S. Eylon, Rev. of Sci. Instrum., Vol. 49, No. 12, p. 1 (1978).


FI